Nonlinear effects of localized absorption perturbations on the light distribution in a turbid medium

Harry L. Graber

Program in Physiology and Biophysics, State University of New York Health Science Center at Brooklyn, Brooklyn, New York 11203

Raphael Aronson

NIR$_x$ Medical Technologies Corporation, West Orange, New Jersey 07052

Randall L. Barbour

Program in Physiology and Biophysics, State University of New York Health Science Center at Brooklyn, Brooklyn, New York 11203, and Department of Pathology, State University of New York Health Science Center at Brooklyn, Brooklyn, New York 11203

Received June 13, 1997; revised manuscript received October 17, 1997; accepted October 27, 1997

A theoretical model of photon propagation in a scattering medium is presented, from which algebraic formulas for the detector-reading perturbations (ΔR) produced by one or two localized perturbations in the macroscopic absorption cross section ($\Delta\mu_a$) are derived. Examination of these shows that when $\Delta\mu_a$ is titrated from very small to large magnitudes in one voxel, the curve traced by the corresponding ΔR values is a rectangular hyperbola. Furthermore, while $\Delta R^{\infty} \equiv \lim_{\Delta\mu_a\to\infty} \Delta R$ is dependent on the location of the detector with respect to the source and the voxel, the ratio $\Delta R/\Delta R^{\infty}$ is independent of the detector location. We also find that when $\Delta\mu_a$ is varied in two voxels simultaneously, the quantity $\Delta R(\Delta\mu_{a,1} \wedge \Delta\mu_{a,2})$ is a bilinear rational function of the $\Delta\mu_a$s. These results apply not only in the case of steady-state illumination and detection but to time-harmonic measurements as well. The validity of the theoretical formulas is demonstrated by applying them to the results of selected numerical diffusion computations. Potential applications of the derived expressions to image-reconstruction problems are discussed.
[S0740-3232(98)01503-8]

OCIS codes: 110.0110, 190.0190, 290.7050.

1. INTRODUCTION

The primary approach we and others have taken in attempting to make the image-recovery problem of photon migration imaging more tractable[1–8] is to recast it as a discrete linear perturbation problem. These methods require specification of a reference medium whose properties are believed to differ as little as possible from those of the target medium. Measurements of both the target and the reference are performed (or estimates thereof are computed), and the differences between corresponding detector readings for the two are the input for the image-recovery algorithm. The media are treated mathematically as sets of discrete voxels. In the linear approximation, each detector reading difference is taken to be a linear combination of the perturbations of the macroscopic absorption and scattering cross sections in all voxels. That is,

$$\Delta R_i = \sum_j w_{ij}\Delta\mu_j , \tag{1.1}$$

where ΔR_i is the change in the ith detector reading, j is an index representing both the voxel and the type of interaction, and the $\Delta\mu_j$'s are the macroscopic cross-section perturbations. The weight w_{ij} is defined as $w_{ij} = -\partial R_i/\partial\mu_j$, where the derivative is evaluated in the absence of the perturbation. As a starting point, for this report we have restricted our attention to effects of perturbations in only the absorption cross section μ_a on the detector readings. In this case, j becomes strictly a voxel index.

When only μ_a is perturbed, Eq. (1.1) can be written in matrix form as $\Delta\mathbf{R} = \mathbf{W}\Delta\boldsymbol{\mu}_a$. When the reference and target media are too dissimilar, then $\mathbf{W}^{-1}\Delta\mathbf{R}$, no matter how accurately computed, is a poor estimate of $\Delta\boldsymbol{\mu}_a$. The reason for this is that nonlinear effects, which come physically from what reactor physicists call "flux depression," enter: the intensity, and thus the absorption rate, is decreased in the vicinity of an absorber. This affects the absorption rate both in the voxel with the increased μ_a and in nearby voxels as well. One can also think of this as a shadowing effect.

A standard approach for dealing with errors of this type is to iteratively update the reference state using Newton-type methods. While this may be effective, the

procedure typically is computation intensive and can be sensitive to noise.[9] Here we have engaged in an effort to consider practical alternative approaches.

We have previously published some numerical studies that indicate that, to a good approximation, nonlinear effects can be taken into account rather simply up to sizable perturbations.[10] This paper presents some theoretical justification of the earlier results, along with further numerical data. The theoretical model for effects of absorption perturbations is given in Section 2, and in Section 3 we use the model to derive formulas for the detector reading perturbation produced either by one or by two localized absorption cross-section perturbations. In Section 4 we compare results of numerical computations to the predictions of the formulas. In Section 5 we discuss the analytical results, and propose two protocols for possibly incorporating corrections for the nonlinear effects into image-reconstruction algorithms.

2. THEORETICAL MODEL

2.A. Steady-State Illumination, Isotropic Scattering

For conceptual simplicity, we restrict our attention at first to the problem of determining the steady-state intensity in a finite medium that may be structurally heterogeneous but in which the differential scattering cross section is everywhere isotropic. Generalization of the model to the frequency domain and to anisotropic scattering will be made later.

Let the medium be subdivided into some number I of voxels. We assume no interactions other than absorption and elastic scattering occur and that a scattered photon may either escape across a boundary of the medium without having another collision or have a subsequent collision in any one of the I voxels. Let P_{ij} be the intensity of light having its first collision in voxel i after being born isotropically and with unit intensity in voxel j. Typically, P_{ij} rapidly decreases as the optical distance between i and j increases. Let φ_i and ϕ_i be, respectively, the unscattered and steady-state intensities in voxel i. Also let $\mathbf{P}$ be the matrix whose ijth element is P_{ij}, and $\boldsymbol{\varphi}$ and $\boldsymbol{\phi}$ be the vectors whose ith elements respectively are φ_i and ϕ_i. Then we have

$$\boldsymbol{\phi} = \sum_{n=0}^{\infty} \mathbf{P}^n \boldsymbol{\varphi}, \tag{2.A.1}$$

where by definition $\mathbf{P}^0 = \mathbf{I}$. The necessary and sufficient condition for convergence is that the absolute value of the largest eigenvalue of $\mathbf{P}$ be less than unity.[11] In the case under consideration, every element of $\mathbf{P}$ is real and nonnegative, which guarantees that the largest eigenvalue is real and positive.[11] $\mathbf{P}$ also has the property that each column sum is strictly less than unity (even if there is no absorption, since any real medium is finite so some photons escape). These properties together are sufficient (but not necessary) to guarantee that the largest eigenvalue is less than unity.[12,13] Thus the series converges, and

$$\boldsymbol{\phi} = (\mathbf{I} - \mathbf{P})^{-1} \boldsymbol{\varphi} \equiv \mathbf{T} \boldsymbol{\varphi}. \tag{2.A.2}$$

In an alternative algebraic approach that does not make use of a collision expansion, we begin by simply defining $\mathbf{P}$ and $\mathbf{T}$ as, respectively, the single-collision and steady-state transfer operators. By definition, in a steady state one additional collision produces no change in the intensity. Thus $\mathbf{P}$ and $\mathbf{T}$ must satisfy the relation $\mathbf{T} = \mathbf{I} + \mathbf{PT}$, from which Eq. (2.A.2) follows directly. Under the conditions posited, a unique inverse of $\mathbf{I} - \mathbf{P}$ exists.

2.B. Extension to Time-Harmonic Illumination

The formulas derived above hold not only in a steady state but also in the frequency domain, so they apply to photon density waves as well. Let the medium be illuminated by a time-dependent source, and define $P_{ij}(t)$, $T_{ij}(t)$, and $\varphi_j(t)$ as rates. Thus $P_{ij}(t)$, for instance, is the intensity per unit time of light having its first collision at time t in voxel i after being born isotropically and with unit intensity in voxel j. We further define $P_{ij}^n(t)$ as the intensity per unit time of light having its nth collision at time t in voxel i after being born isotropically and with unit intensity in voxel j. From these definitions it follows that $P_{ij}^n(t)$ is a convolution in time and a sum over all voxels in which the previous collision could have taken place:

$$P_{ij}^n(t) = \sum_{k=1}^{I} \left[\int_0^t P_{ik}(t') P_{kj}^{n-1}(t - t') \mathrm{d}t' \right]. \tag{2.B.1}$$

Note that $\mathbf{P}$ can be recast as a product $\mathbf{P} = \mathbf{QS}$, where the time-of-flight dependence resides only in $\mathbf{Q}$, while $\mathbf{S}$ is a diagonal matrix involving only the cross sections, which are time independent. Thus $\mathbf{S}$ is independent of frequency [put another way, $\mathbf{S}(t)$ is a δ-function in time, since an absorption is essentially instantaneous], so $\mathbf{P}(\omega) = \mathbf{Q}(\omega)\mathbf{S}$. Then all the equations we derive explicitly in the steady-state case continue to hold in the frequency domain. Thus, in the frequency domain Eq. (2.B.1) becomes a product relation, which when written in matrix form is

$$\mathbf{P}^n(\omega) = \mathbf{P}(\omega)\mathbf{P}^{n-1}(\omega). \tag{2.B.2}$$

Since by definition $\mathbf{P}^0(\omega) = \mathbf{I}$, $\mathbf{P}^n(\omega) = [\mathbf{P}(\omega)]^n$.

Let t_{ij} be the time it takes for a photon to get from some point in voxel j to some point in voxel i without collision. Then $\mathbf{P}(t) = \mathbf{P}\delta(t - t_{ij})$, where $\mathbf{P}$ is the steady-state matrix, so the Fourier transform of $\mathbf{P}(t)$ is

$$\mathbf{P}(\omega) = \int_{-\infty}^{\infty} \mathbf{P}(t) \exp(-i\omega t) \mathrm{d}t = \mathbf{P} \exp(-i\omega t_{ij}). \tag{2.B.3}$$

The uncertainty in the phase is quite small with the voxels we consider, whose dimensions are on the order of one transport mean free pathlength. This is $\sim$1 mm for near-infrared radiation in tissue, so if we take the uncertainty in path length to be 1 mm, the corresponding uncertainty in time for a speed of 2×10^8 m-s^{-1} is $\Delta t = 5 \times 10^{-12}$ s. At a modulation frequency of 200 MHz, $\omega \Delta t = 2\pi \times 10^{-3}$ radians, or about 1/3 of a degree, which for practical purposes is negligible.

2.C. Anisotropic Scattering and Flux Computations

When the scattering is anisotropic, there is a correlation between the direction in which a photon enters a scatter-

ing interaction and the direction in which it leaves. It is therefore necessary to discretize the medium in direction as well as in position. Thus the elements of the corresponding **P** matrix would be indexed by both voxel and direction numbers. With this modification, the above formalism remains valid.

Indexing in direction as well as position would lead to a **T** matrix from which we could compute photon fluxes as well as intensities. Thus it could be worthwhile to perform the direction discretization even in the isotropic-scattering case.

3. ABSORPTION-CROSS-SECTION PERTURBATIONS

3.A. General Formalism

The formalism we will start from in our analyses of the effects of localized absorption perturbations on the collision rate is well known in scattering theory, and it has been used in some theoretical work on optical tomography.[14,15] Consider the **P** and **T** matrices for some medium, let $\mathbf{P}_0$ and $\mathbf{T}_0$ be the corresponding matrices for a different medium, which we will think of as the background, and let $\Delta\mathbf{P} = \mathbf{P} - \mathbf{P}_0$. If $\mathbf{T}_0 = (\mathbf{I} - \mathbf{P}_0)^{-1}$ and $\mathbf{T} = (\mathbf{I} - \mathbf{P})^{-1}$, we have $(\mathbf{I} - \mathbf{P}_0)(\mathbf{T} - \mathbf{T}_0)(\mathbf{I} - \mathbf{P}) = (\mathbf{I} - \mathbf{P}_0) - (\mathbf{I} - \mathbf{P}) = \Delta\mathbf{P}$, so that $\mathbf{T} - \mathbf{T}_0 = \mathbf{T}_0\Delta\mathbf{P}\mathbf{T}$. Left-multiplying by $\Delta\mathbf{P}$ and reassociating terms gives $\Delta\mathbf{P}\mathbf{T} = \Delta\mathbf{P}\mathbf{T}_0 + \Delta\mathbf{P}\mathbf{T}_0\Delta\mathbf{P}\mathbf{T}$, from which it follows that $\Delta\mathbf{P}\mathbf{T} = (\mathbf{I} - \Delta\mathbf{P}\mathbf{T}_0)^{-1}\Delta\mathbf{P}\mathbf{T}_0$. Thus, finally,

$$\mathbf{T} = \mathbf{T}_0 + \mathbf{T}_0(\mathbf{I} - \Delta\mathbf{P}\mathbf{T}_0)^{-1}\Delta\mathbf{P}\mathbf{T}_0. \tag{3.A.1}$$

This formula is totally general, i.e., no assumptions were made about the form of $\Delta\mathbf{P}$. In Subsections 3.B–3.D, we will make an approximation in which **T** is of the form $\mathbf{T} = (\mathbf{I} - \mathbf{P}_0\mathbf{X})^{-1}$, where **X** is a diagonal matrix. Defining $\mathbf{Y} = \mathbf{I} - \mathbf{X}$ and substituting $-\mathbf{P}_0\mathbf{Y}$ for $\Delta\mathbf{P}$ gives

$$\begin{aligned}\mathbf{T} &= \mathbf{T}_0 - \mathbf{T}_0(\mathbf{I} + \mathbf{P}_0\mathbf{Y}\mathbf{T}_0)^{-1}\mathbf{P}_0\mathbf{Y}\mathbf{T}_0 \\ &= \mathbf{T}_0 - \mathbf{T}_0\mathbf{P}_0\mathbf{Y}(\mathbf{I} + \mathbf{T}_0\mathbf{P}_0\mathbf{Y})^{-1}\mathbf{T}_0.\end{aligned} \tag{3.A.2}$$

The third form follows from the second, since $\mathbf{a}(\mathbf{I} + \mathbf{b}\mathbf{a}) = \mathbf{a} + \mathbf{a}\mathbf{b}\mathbf{a} = (\mathbf{I} + \mathbf{a}\mathbf{b})\mathbf{a} \Rightarrow (\mathbf{I} + \mathbf{a}\mathbf{b})^{-1}\mathbf{a} = \mathbf{a}(\mathbf{I} + \mathbf{b}\mathbf{a})^{-1}$. We will show below that detector-reading perturbations are functions of the matrix $\mathbf{T}_0 - \mathbf{X}\mathbf{T}$, which according to Eq. (3.A.2) is

$$\mathbf{T}_0 - \mathbf{X}\mathbf{T} = \mathbf{Y}\mathbf{T}_0 + (\mathbf{I} - \mathbf{Y})\mathbf{T}_0\mathbf{P}_0\mathbf{Y}(\mathbf{I} + \mathbf{T}_0\mathbf{P}_0\mathbf{Y})^{-1}\mathbf{T}_0. \tag{3.A.3}$$

3.B. Detector Readings: Lattice versus Continuum Models

A detector reading is of the form

$$R = \sum_{i=1}^{I} r_i\phi_i = \mathbf{r}^T\boldsymbol{\phi}, \tag{3.B.1}$$

where r_i is the response of the detector to the last-time-scattered intensity in voxel i. Now consider this relation for both a perturbed and an unperturbed system. For the unperturbed system we will put a subscript or superscript 0 on the relevant vectors and matrices; the perturbed system will be referred to without sub/superscripts. The perturbations considered will be changes $\Delta\mu_{a,k}$ in the absorption cross sections in some set of voxels.

A basic assumption we make is that the perturbation in $\mu_{a,k}$ does not have any effect on any of the elements of the unscattered intensity vector $\boldsymbol{\varphi}$. This would be exactly true if, for example, a line source were used and the perturbed voxels did not lie on the source line; it would be significantly violated only if some perturbed voxels lay at or near the site where the source was incident on the medium. In the same spirit, we assume that the perturbation in $\mu_{a,k}$ does not have any effect on any of the elements of **r**. The model used to generate the illustrative data presented in this paper satisfies these assumptions, but in the end their validity must be tested numerically and experimentally.

For the unperturbed system, we have detector reading

$$R_0 = \mathbf{r}_0^{\mathrm{T}}\mathbf{T}_0\boldsymbol{\varphi}^0, \tag{3.B.2}$$

where, as developed above in Section 2, $\mathbf{T}_0 = (\mathbf{I} - \mathbf{P}_0)^{-1}$. For the perturbed system, we draw a distinction between two cases, lattice models and continuum models of photon transport.

In a lattice model, such as the one we used to generate our illustrative data, transitions occur only between adjacent lattice points. The matrix element P_{ij} has in it a factor $\mu_{s,j}/\mu_{t,j}$, the scattering probability in voxel j. If we change the absorption cross section in voxel j, with $\mu_{a,j} \to \mu_{a,j} + \Delta\mu_{a,j}$, we have

$$\frac{\mu_{s,j}}{\mu_{t,j}} = \frac{\mu_{s,j}}{\mu_{t,j}^0}\frac{\mu_{t,j}^0}{\mu_{t,j}} = \frac{\mu_{s,j}}{\mu_{t,j}^0}\frac{\mu_{t,j}^0}{\mu_{t,j}^0 + \Delta\mu_{a,j}} \equiv \frac{\mu_{s,j}}{\mu_{t,j}^0}x_j. \tag{3.B.3}$$

Let us define the matrix **X** with elements $X_{ij} = x_j\delta_{ij}$. Also, unlike a continuous medium, where there is an unambiguous, natural definition for intensity, in a lattice model there is an unavoidable element of arbitrariness in the definition. Here we define $\boldsymbol{\varphi}$ in terms of the number of photons entering the lattice cells. Then $\mathbf{P} = \mathbf{P}_0\mathbf{X}$ (it would be $\mathbf{X}\mathbf{P}_0$ if we had defined $\boldsymbol{\varphi}$ in terms of the number of photons leaving the lattice cells), and

$$R = \mathbf{r}^{\mathrm{T}}\mathbf{X}\mathbf{T}\boldsymbol{\varphi} = \mathbf{r}^{\mathrm{T}}\mathbf{X}(\mathbf{I} - \mathbf{P}_0\mathbf{X})^{-1}\boldsymbol{\varphi}. \tag{3.B.4}$$

The **X** to the left of the **T** in Eq. (3.B.4) arises from the fact that photons arriving at the detector have one more collision in the last voxel.

In the continuum case, the ratios of scattering to total cross sections do not appear explicitly as multiplicative factors in **P**. Rather, there is additional attenuation in each affected voxel. An additional basic assumption that we make here, which does not arise in the lattice case (where all free paths are between nearest neighbors), is that P_{ij} is affected by a perturbation in either $\mu_{a,j}$ or $\mu_{a,i}$ but that the effect on P_{ij} of perturbations in voxels that a photon must cross in getting from voxel j to voxel i may be safely ignored. We believe the results derived under this assumption are qualitatively correct, because (A) given a perturbation in voxel k, only a small fraction of voxel pairs in the medium have voxel k on the direct path between them; (B) given the typically rapid decrease in P_{ij} with increasing distance between voxels i and j, few of the affected elements of **P** are significantly greater than

zero in any case; (C) both voxels in every pair that *does* sit astride the perturbed voxel receive the bulk of their total intensity from other, unperturbed voxels.

Perhaps the most reasonable expression for the additional attenuation factor in voxel k is

$$x_k = \exp(-\Delta\mu_{a,k}\ell_k), \tag{3.B.5}$$

where ℓ_k is a distance taken to be on the order of the linear dimension of the voxel. Although arguments can be advanced for making ℓ_k either smaller than or larger than the voxel dimension, that certainly is approximately correct. Although we will continue, for reasons of notational convenience, to define $\mathbf{P}$ as $\mathbf{P}_0\mathbf{X}$, the quantity that should replace $\mathbf{P}_0$ in the expression for R is

$$\mathbf{P}' = \mathbf{X}^{1/2}\mathbf{P}_0\mathbf{X}^{1/2}, \tag{3.B.6}$$

where $(\mathbf{X}^{1/2})_{ij} = \sqrt{x_j}\delta_{ij}$. The rationale for this is that on average a photon is attenuated by an extra factor $\exp(-\Delta\mu_{a,i}\ell_i/2)$ if there is a perturbation in voxel i and by $\exp(-\Delta\mu_{a,j}\ell_j/2)$ if there is a perturbation in voxel j. This rationale should hold irrespective of the choice we ultimately make for the form of x_k.

The detector-reading perturbation $\Delta R = R_0 - R$ will be a rational function of the $\Delta\mu_a$'s in a lattice model. In a continuum model, one can replace Eq. (3.B.5) by a rational function that goes to the same limits when $\Delta\mu_a$ goes to either zero or infinity, and that has the same derivative as $\Delta\mu_a$ goes to zero. The simplest such expression is

$$x_k \approx \frac{1}{1 + \Delta\mu_{a,k}\ell_k}. \tag{3.B.7}$$

However, none of the subsequent discussion depends on making this approximation.

With the definitions we are using, two other changes must be made in a continuum model vis-à-vis a lattice model when the absorption cross section is perturbed. First, $\boldsymbol{\varphi}$ must be replaced by $\mathbf{X}^{1/2}\boldsymbol{\varphi}$ because on the average an unscattered photon penetrates halfway into the first-collision voxel before having the first collision. Second, $\boldsymbol{\phi}$ must be replaced by $\mathbf{X}^{1/2}\boldsymbol{\phi}$ because on the average a photon must travel halfway through the last-collision voxel after the last collision before it reaches the detector at the surface. Thus we replace Eq. (3.B.4) with

$$R = \mathbf{r}^{\mathrm{T}}\mathbf{X}^{1/2}(\mathbf{I} - \mathbf{X}^{1/2}\mathbf{P}_0\mathbf{X}^{1/2})^{-1}\mathbf{X}^{1/2}\boldsymbol{\varphi}. \tag{3.B.8}$$

Now, $\mathbf{X}^{1/2}(\mathbf{I} - \mathbf{X}^{1/2}\mathbf{P}_0\mathbf{X}^{1/2})^{-1}\mathbf{X}^{1/2} = [\mathbf{X}^{-1/2}(\mathbf{I} - \mathbf{X}^{1/2}\mathbf{P}_0\mathbf{X}^{1/2})\mathbf{X}^{-1/2}]^{-1} = [(\mathbf{I} - \mathbf{P}_0\mathbf{X})\mathbf{X}^{-1}]^{-1} = \mathbf{X}(\mathbf{I} - \mathbf{P}_0\mathbf{X})^{-1}$. Using our previous definition, $\mathbf{T} = (\mathbf{I} - \mathbf{P}_0\mathbf{X})^{-1}$, gives the same formal result as in the lattice model: $R = \mathbf{r}^{\mathrm{T}}\mathbf{X}\mathbf{T}\boldsymbol{\varphi}$.

With these definitions, then, from either a lattice model or a continuum model the detector-reading perturbation is $\Delta R = \mathbf{r}_0^{\mathrm{T}}\mathbf{T}_0\boldsymbol{\varphi}^0 - \mathbf{r}^{\mathrm{T}}\mathbf{X}\mathbf{T}\boldsymbol{\varphi}$. As we are assuming that $\boldsymbol{\varphi} = \boldsymbol{\varphi}^0$ and that $\mathbf{r}^{\mathrm{T}} = \mathbf{r}_0^{\mathrm{T}}$, we have

$$\Delta R = \mathbf{r}_0^{\mathrm{T}}(\mathbf{T}_0 - \mathbf{X}\mathbf{T})\boldsymbol{\varphi}^0. \tag{3.B.9}$$

Let $\mathbf{Y} = \mathbf{I} - \mathbf{X}$ and let $y_j = 1 - x_j$, so that $Y_{ij} = y_j\delta_{ij}$. Only those y_i's corresponding to perturbed voxels are nonzero. Now, $\mathbf{Y} = \mathbf{I} - \mathbf{P}_0\mathbf{X} - \mathbf{X} + \mathbf{P}_0\mathbf{X} = (\mathbf{I} - \mathbf{P}_0\mathbf{X}) - (\mathbf{I} - \mathbf{P}_0)\mathbf{X} = \mathbf{T}^{-1} - \mathbf{T}_0^{-1}\mathbf{X} = \mathbf{T}_0^{-1}(\mathbf{T}_0 - \mathbf{X}\mathbf{T})\mathbf{T}^{-1}$, or

$$\mathbf{T}_0 - \mathbf{X}\mathbf{T} = \mathbf{T}_0\mathbf{Y}\mathbf{T}. \tag{3.B.10}$$

Then $\mathbf{T}_0 = (\mathbf{X} + \mathbf{T}_0\mathbf{Y})\mathbf{T} = (\mathbf{I} - \mathbf{Y} + \mathbf{T}_0\mathbf{Y})\mathbf{T} = (\mathbf{Y}^{-1} - \mathbf{I} + \mathbf{T}_0)\mathbf{Y}\mathbf{T}$. Let $\mathbf{V} \equiv \mathbf{Y}^{-1} - \mathbf{I} + \mathbf{T}_0$. That is,

$$\mathbf{T}_0 = \mathbf{V}\mathbf{Y}\mathbf{T}. \tag{3.B.11}$$

3.C. Absorption Perturbed in Exactly One Voxel

Let us perturb a single voxel, which we will call q, by altering only its absorption cross section. So only the qqth element of $\mathbf{Y}$ is nonzero, and Eqs. (3.B.10) and (3.B.11) give us $(\mathbf{T}_0 - \mathbf{X}\mathbf{T})_{ij} = (\mathbf{T}_0)_{iq}(\mathbf{Y}\mathbf{T})_{qj}$ and $(\mathbf{T}_0)_{qj} = V_{qq}(\mathbf{Y}\mathbf{T})_{qj}$, respectively. Combining these relations leads to

$$(\mathbf{T}_0 - \mathbf{X}\mathbf{T})_{ij} = \frac{(\mathbf{T}_0)_{iq}(\mathbf{T}_0)_{qj}}{V_{qq}}, \tag{3.C.1}$$

and substitution of Eq. (3.C.1) into Eq. (3.B.9) gives us

$$\begin{aligned}\Delta R &= \frac{1}{V_{qq}}\sum_{i,j} r_{0,i}(\mathbf{T}_0)_{iq}(\mathbf{T}_0)_{qj}\varphi_j^0 \\ &= \frac{1}{V_{qq}}\left[\sum_i r_{0,i}(\mathbf{T}_0)_{iq}\right]\left[\sum_j (\mathbf{T}_0)_{qj}\varphi_j^0\right] \\ &= \frac{1}{V_{qq}}\left[\sum_i r_{0,i}(\mathbf{T}_0)_{iq}\right]\phi_q^0 = \frac{\mathbf{r}_0^{\mathrm{T}}\mathbf{t}_q\phi_q^0}{V_{qq}},\end{aligned} \tag{3.C.2}$$

where $\mathbf{t}_q$ is the qth column of $\mathbf{T}_0$, $(\mathbf{t}_q)_i = (\mathbf{T}_0)_{iq}$. Now $V_{qq} = y_q^{-1} - 1 + (\mathbf{T}_0)_{qq}$, and so

$$\Delta R = \frac{\mathbf{r}_0^{\mathrm{T}}\mathbf{t}_q\phi_q^0 y_q}{1 + (\mathbf{T}_0 - \mathbf{I})_{qq}y_q}, \tag{3.C.3}$$

which is a rational function in y_q. For the lattice and continuum cases we have, respectively, $y_q = \Delta\mu_{a,q}/(\mu_{t,q}^0 + \Delta\mu_{a,q})$ and $y_q \approx \Delta\mu_{a,q}/(\ell_q^{-1} + \Delta\mu_{a,q})$. Then the detector-reading perturbation is

$$\Delta R = \frac{\mathbf{r}_0^{\mathrm{T}}\mathbf{t}_q\phi_q^0\Delta\mu_{a,q}}{\mu_{t,q}^0 + (\mathbf{T}_0)_{qq}\Delta\mu_{a,q}} \tag{3.C.4a}$$

for the lattice case, and

$$\Delta R \approx \frac{\mathbf{r}_0^{\mathrm{T}}\mathbf{t}_q\phi_q^0\Delta\mu_{a,q}}{\frac{1}{\ell_q} + (\mathbf{T}_0)_{qq}\Delta\mu_{a,q}} \tag{3.C.4b}$$

for the continuum case. Each of these is a simple rational function in which the numerator and denominator are both linear in $\Delta\mu_{a,q}$.

The greatest possible detector-reading perturbation that can be caused by an absorption perturbation in voxel q is

$$\Delta R^{\infty_q} \equiv \lim_{\Delta\mu_{a,q}\to\infty}\Delta R = \frac{\mathbf{r}_0^{\mathrm{T}}\mathbf{t}_q\phi_q^0}{(\mathbf{T}_0)_{qq}}, \tag{3.C.5}$$

while the limiting (linear) form for small absorption perturbations is

$$\lim_{\Delta\mu_{a,q}\to 0}\Delta R = \frac{\mathbf{r}_0^{\mathrm{T}}\mathbf{t}_q\phi_q^0}{\kappa_q}\Delta\mu_{a,q}, \tag{3.C.6}$$

where κ_q is either $\mu_{t,q}^0$ (lattice case) or ℓ_q^{-1} (continuum case). This gives the linear absorption weight of the jth voxel for the ith detector [Eq. (1.1)],

$$w_{ij} = \frac{\mathbf{r}_{0,i}^{\mathrm{T}} \mathbf{t}_j \phi_j^0}{\kappa_j}, \tag{3.C.7}$$

where we use $\mathbf{r}_{0,i}$ to denote the ith detector's response function.

From Eqs. (3.C.4) and (3.C.5), one has

$$\frac{\Delta R}{\Delta R^{\infty_q}} = \frac{\Delta \mu_{a,q}}{\dfrac{\kappa_q}{(\mathbf{T}_0)_{qq}} + \Delta \mu_{a,q}}. \tag{3.C.8}$$

There is no dependence on the detector response function $\mathbf{r}_0$ in Eq. (3.C.8), so the ratio $\Delta R/\Delta R^{\infty_q}$ is independent of detector location. Furthermore, its dependence on the location of the perturbed voxel will be weak to the extent that $\kappa_q/(\mathbf{T}_0)_{qq}$ is slowly spatially varying.

From Eqs. (3.C.5) and (3.C.7), one has

$$\frac{\Delta R_i^{\infty_j}}{w_{ij}} = \frac{\kappa_j}{(\mathbf{T}_0)_{jj}}, \tag{3.C.9}$$

in which there is, again, no dependence on the detector location. This fact may be useful when attempting to incorporate a correction for the nonlinear dependence of detector readings on absorption perturbations into an image reconstruction procedure (see Subsection 5.D).

3.D. Absorption Perturbed in Exactly Two Voxels

Let us perturb two voxels, which we will call q and p, by altering only their absorption cross sections. So only the qqth and ppth elements of $\mathbf{Y}$ are nonzero, and Eq. (3.B.10) gives us $(\mathbf{T}_0 - \mathbf{XT})_{ij} = (\mathbf{T}_0)_{iq}(\mathbf{YT})_{qj} + (\mathbf{T}_0)_{ip}(\mathbf{YT})_{pj}$. And from Eq. (3.B.11),

$$\begin{aligned}(\mathbf{T}_0)_{qj} &= V_{qq}(\mathbf{YT})_{qj} + (\mathbf{T}_0)_{qp}(\mathbf{YT})_{pj},\\ (\mathbf{T}_0)_{pj} &= V_{pp}(\mathbf{YT})_{pj} + (\mathbf{T}_0)_{pq}(\mathbf{YT})_{qj}.\end{aligned} \tag{3.D.1}$$

Inverting Eq. (3.D.1) yields

$$\begin{aligned}(\mathbf{YT})_{qj} &= \frac{1}{\Delta}[V_{pp}(\mathbf{T}_0)_{qj} - (\mathbf{T}_0)_{qp}(\mathbf{T}_0)_{pj}],\\ (\mathbf{YT})_{pj} &= \frac{1}{\Delta}[V_{qq}(\mathbf{T}_0)_{pj} - (\mathbf{T}_0)_{pq}(\mathbf{T}_0)_{qj}],\end{aligned} \tag{3.D.2}$$

where $\Delta \equiv V_{qq}V_{pp} - (\mathbf{T}_0)_{qp}(\mathbf{T}_0)_{pq}$. Substitution of Eq. (3.D.2) into the expression for $(\mathbf{T}_0 - \mathbf{XT})_{ij}$ results in

$$(\mathbf{T}_0 - \mathbf{XT})_{ij} = \frac{(\mathbf{T}_0)_{iq}[V_{pp}(\mathbf{T}_0)_{qj} - (\mathbf{T}_0)_{qp}(\mathbf{T}_0)_{pj}] + (\mathbf{T}_0)_{ip}[V_{qq}(\mathbf{T}_0)_{pj} - (\mathbf{T}_0)_{pq}(\mathbf{T}_0)_{qj}]}{\Delta}. \tag{3.D.3}$$

Next, substitution of Eq. (3.D.3) into Eq. (3.B.9) gives us

$$\Delta R = \mathbf{r}_0^{\mathrm{T}} \frac{\mathbf{t}_q V_{pp}\phi_q^0 + \mathbf{t}_p V_{qq}\phi_p^0 - \mathbf{t}_q(\mathbf{T}_0)_{qp}\phi_p^0 - \mathbf{t}_p(\mathbf{T}_0)_{pq}\phi_q^0}{\Delta}. \tag{3.D.4}$$

When rewritten in terms of y_q and y_p, Eq. (3.D.4) becomes

$$\begin{aligned}\Delta R &= \mathbf{r}_0^{\mathrm{T}} \frac{\mathbf{t}_q\phi_q^0 y_q + \mathbf{t}_p\phi_p^0 y_p + A_{q,p}y_q y_p}{1 + (\mathbf{T}_0 - \mathbf{I})_{qq}y_q + (\mathbf{T}_0 - \mathbf{I})_{pp}y_p + B_{q,p}y_q y_p},\\ A_{q,p} &= \mathbf{t}_q(\mathbf{T}_0 - \mathbf{I})_{pp}\phi_q^0 + \mathbf{t}_p(\mathbf{T}_0 - \mathbf{I})_{qq}\phi_p^0 - \mathbf{t}_q(\mathbf{T}_0)_{qp}\phi_p^0\\ &\quad - \mathbf{t}_p(\mathbf{T}_0)_{pq}\phi_q^0,\\ B_{q,p} &= (\mathbf{T}_0 - \mathbf{I})_{qq}(\mathbf{T}_0 - \mathbf{I})_{pp} - (\mathbf{T}_0)_{qp}(\mathbf{T}_0)_{pq}.\end{aligned} \tag{3.D.5}$$

For the lattice case, we define $z \equiv \Delta\mu_{a,q}/\mu_{t,q}^0$ and $\nu \equiv \Delta\mu_{a,p}/\mu_{t,p}^0$; for the continuum case the definitions are $z \equiv \Delta\mu_{a,q}\ell_q$ and $\nu \equiv \Delta\mu_{a,p}\ell_p$. In either case we have $y_q = z/(1+z)$ and $y_p = \nu/(1+\nu)$. Substituting these expressions into Eq. (3.D.5), we get

$$\Delta R = \mathbf{r}_0^{\mathrm{T}} \frac{\mathbf{t}_q\phi_q^0 z + \mathbf{t}_p\phi_p^0\nu + [\mathbf{t}_q(\mathbf{T}_0)_{pp}\phi_q^0 + \mathbf{t}_p(\mathbf{T}_0)_{qq}\phi_p^0 - \mathbf{t}_q(\mathbf{T}_0)_{qp}\phi_p^0 - \mathbf{t}_p(\mathbf{T}_0)_{pq}\phi_q^0]z\nu}{1 + (\mathbf{T}_0)_{qq}z + (\mathbf{T}_0)_{pp}\nu + [(\mathbf{T}_0)_{qq}(\mathbf{T}_0)_{pp} - (\mathbf{T}_0)_{qp}(\mathbf{T}_0)_{pq}]z\nu}. \tag{3.D.6}$$

Thus ΔR is a rational function in which both numerator and denominator are bilinear in $\Delta\mu_{a,q}$ and $\Delta\mu_{a,p}$. As required, Eq. (3.D.6) is invariant under exchange of the indices p and q. Also, when $\Delta\mu_{a,p} = 0$, Eq. (3.D.6) reduces to Eq. (3.C.4).

The interaction between the two absorption perturbations can be quantified by comparing Eq. (3.D.6) to the detector-reading perturbation that would result if their effects were simply additive. In that case the combined effect would be

$$\Delta R = \mathbf{r}_0^{\mathrm{T}} \frac{\mathbf{t}_q\phi_q^0 z + \mathbf{t}_p\phi_p^0\nu + [\mathbf{t}_q(\mathbf{T}_0)_{pp}\phi_q^0 + \mathbf{t}_p(\mathbf{T}_0)_{qq}\phi_p^0]z\nu}{1 + (\mathbf{T}_0)_{qq}z + (\mathbf{T}_0)_{pp}\nu + (\mathbf{T}_0)_{qq}(\mathbf{T}_0)_{pp}z\nu}. \tag{3.D.7}$$

We see immediately that the difference between Eqs. (3.D.6) and (3.D.7) is that the latter contains only the diagonal elements of $\mathbf{T}_0$ and lacks the off-diagonal elements. It is to be expected that $(\mathbf{T}_0)_{qp}$ and $(\mathbf{T}_0)_{pq}$ will typically decrease as the distance between voxels p and q increases. As this happens the mutual coupling effect will likewise diminish, so Eq. (3.D.7) is a limiting form of Eq. (3.D.6). The mutual coupling is the difference between Eq. (3.D.7) and Eq. (3.D.6). The relative mutual coupling $1 - [\Delta R^{pq}/(\Delta R^q + \Delta R^p)]$ is, however, frequently a more useful quantity for describing the effect. For either the absolute or the relative mutual coupling, the equations give rise to a rational function containing terms up to $z^2\nu^2$ in both numerator and denominator. As required, its value is exactly zero if either $\Delta\mu_{a,q} = 0$ or $\Delta\mu_{a,p} = 0$. The coefficients for both functions are given in Table 1.

In contrast to the single-absorber case, here the nor-

Table 1. Coefficients of Rational Functions for the Absolute Mutual Coupling $\Delta R^q + \Delta R^p - \Delta R^{pq}$ and the Relative Mutual Coupling $1 - [\Delta R^{pq}/(\Delta R^q + \Delta R^p)]$ between Two Perturbed Voxels (See Subsection 3.D), in Terms of the Relative Absorption Perturbations z and ν

Coefficient Multiplying	Numerator	Denominator, Absolute Mutual Coupling	Denominator, Relative Mutual Coupling
1	0	1	0
z	0	$2(\mathbf{T}_0)_{qq}$	$\mathbf{r}_0^{\mathrm{T}}\mathbf{t}_q\phi_q^0$
ν	0	$2(\mathbf{T}_0)_{pp}$	$\mathbf{r}_0^{\mathrm{T}}\mathbf{t}_p\phi_p^0$
z^2	0	$(\mathbf{T}_0)_{qq}^2$	$\mathbf{r}_0^{\mathrm{T}}\mathbf{t}_q(\mathbf{T}_0)_{qq}\phi_q^0$
ν^2	0	$(\mathbf{T}_0)_{pp}^2$	$\mathbf{r}_0^{\mathrm{T}}\mathbf{t}_p(\mathbf{T}_0)_{pp}\phi_p^0$
$z\nu$	$\mathbf{r}_0^{\mathrm{T}}[\mathbf{t}_q(\mathbf{T}_0)_{qp}\phi_p^0 + \mathbf{t}_p(\mathbf{T}_0)_{pq}\phi_q^0]$	$4(\mathbf{T}_0)_{qq}(\mathbf{T}_0)_{pp} - (\mathbf{T}_0)_{qp}(\mathbf{T}_0)_{pq}$	$2\mathbf{r}_0^{\mathrm{T}}[\mathbf{t}_q(\mathbf{T}_0)_{pp}\phi_q^0 + \mathbf{t}_p(\mathbf{T}_0)_{qq}\phi_p^0]$
$z^2\nu$	$\mathbf{r}_0^{\mathrm{T}}[\mathbf{t}_q(\mathbf{T}_0)_{qq}(\mathbf{T}_0)_{qp}\phi_p^0 + \mathbf{t}_p(\mathbf{T}_0)_{pq}(\mathbf{T}_0)_{qq}\phi_q^0 - \mathbf{t}_q(\mathbf{T}_0)_{qp}(\mathbf{T}_0)_{pq}\phi_q^0]$	$(\mathbf{T}_0)_{qq}[2(\mathbf{T}_0)_{qq}(\mathbf{T}_0)_{pp} - (\mathbf{T}_0)_{qp}(\mathbf{T}_0)_{pq}]$	$\mathbf{r}_0^{\mathrm{T}}[2\mathbf{t}_q(\mathbf{T}_0)_{qq}(\mathbf{T}_0)_{pp}\phi_q^0 + \mathbf{t}_p(\mathbf{T}_0)_{qq}^2\phi_p^0 - \mathbf{t}_q(\mathbf{T}_0)_{qp}(\mathbf{T}_0)_{pq}\phi_q^0]$
$z\nu^2$	$\mathbf{r}_0^{\mathrm{T}}[\mathbf{t}_p(\mathbf{T}_0)_{pp}(\mathbf{T}_0)_{pq}\phi_q^0 + \mathbf{t}_q(\mathbf{T}_0)_{qp}(\mathbf{T}_0)_{pp}\phi_p^0 - \mathbf{t}_p(\mathbf{T}_0)_{pq}(\mathbf{T}_0)_{qp}\phi_p^0]$	$(\mathbf{T}_0)_{pp}[2(\mathbf{T}_0)_{qq}(\mathbf{T}_0)_{pp} - (\mathbf{T}_0)_{qp}(\mathbf{T}_0)_{pq}]$	$\mathbf{r}_0^{\mathrm{T}}[2\mathbf{t}_p(\mathbf{T}_0)_{qq}(\mathbf{T}_0)_{pp}\phi_p^0 + \mathbf{t}_q(\mathbf{T}_0)_{pp}^2\phi_p^0 - \mathbf{t}_p(\mathbf{T}_0)_{pq}(\mathbf{T}_0)_{qp}\phi_q^0]$
$z^2\nu^2$	$\mathbf{r}_0^{\mathrm{T}}\{\mathbf{t}_q(\mathbf{T}_0)_{qp}(\mathbf{T}_0)_{pp}[(\mathbf{T}_0)_{qq}\phi_p^0 - (\mathbf{T}_0)_{pq}\phi_q^0] + \mathbf{t}_p(\mathbf{T}_0)_{pq}(\mathbf{T}_0)_{qq}[(\mathbf{T}_0)_{pp}\phi_q^0 - (\mathbf{T}_0)_{qp}\phi_p^0]\}$	$(\mathbf{T}_0)_{qq}(\mathbf{T}_0)_{pp}[(\mathbf{T}_0)_{qq}(\mathbf{T}_0)_{pp} - (\mathbf{T}_0)_{qp}(\mathbf{T}_0)_{pq}]$	$\mathbf{r}_0^{\mathrm{T}}[\mathbf{t}_q(\mathbf{T}_0)_{pp}\phi_q^0 + \mathbf{t}_p(\mathbf{T}_0)_{qq}\phi_p^0] \times [(\mathbf{T}_0)_{qq}(\mathbf{T}_0)_{pp} - (\mathbf{T}_0)_{qp}(\mathbf{T}_0)_{pq}]$

malized detector-reading perturbation is not, in general, the same in all voxels. We have found it is not possible to eliminate all reference to the detector response function from the expression for the ratio of ΔR^{pq} to $\Delta R^{\infty_p\infty_q}$. Therefore the normalized detector-reading perturbation is a function of position within the medium. This is a consequence of having absorption perturbations in two distinct voxels at the same time, and is not caused by their mutual coupling, for the ratio of $\Delta R^q + \Delta R^p$ to $\Delta R^{\infty_p} + \Delta R^{\infty_q}$ also retains a dependence on $\mathbf{r}_0$.

4. ILLUSTRATIVE DATA

4.A. Methods

4.A.1. Relaxation Solver

In order to demonstrate relationships derived in the preceding section, sets of detector readings were computed using a relaxation code.[16] It numerically computes solutions to a six-flux model of light propagation. The media modeled in these computations are, strictly speaking, sets of discrete points or nodes, with each node directly linked to six others. It is conceptually simpler, however, to envision them as continuous three-dimensional media subdivided into cubical cells. Corresponding to each cell is a six-dimensional vector $\mathbf{f}$, each component of which is a discretized angular intensity (or specific intensity, or radiance) in one of the allowed directions.

The relaxation model is an order-of-scattering calculation in which the light is constrained to move exactly one mean free path (mfp) between successive collisions, from the cell it occupies into the six contiguous cells. The propagation of light into a cell from each of its six neighbors is governed by a 6×6 scattering matrix $\mathbf{p}$, where p_{ij} is the fraction of light entering the cell in direction j that scatters into direction i. Any desired type and extent of heterogeneity and anisotropy can be modeled in the relaxation code's most general form, because $\mathbf{p}$ can be independently specified for every cell in the medium, and it need not be symmetric. However, for our purposes we modeled only media that were homogeneous except for one or two cells, with scattering everywhere isotropic, and no internal reflection at the boundaries. Combining the angular intensity vectors and scattering matrices for all the cells into a single system of linear equations gives us $\mathbf{f}(n+1) = \mathbf{P}_{\mathrm{rlx}}\mathbf{f}(n)$. The transmission matrix $\mathbf{P}_{\mathrm{rlx}}$ is the relaxation model equivalent of the direction-discretized one-step transition matrix $\mathbf{P}$ defined in Subsection 2.C. Then $\mathbf{f}(n)$ is $\mathbf{P}_{\mathrm{rlx}}^n\boldsymbol{\varphi}$.

The dimensions of a slab medium, the absorption coefficient of each cell, and a first-collision distribution (i.e., a $\boldsymbol{\varphi}$) are specified at the outset of a computation. The computation terminates when the Euclidean norm $\|\mathbf{f}(n)\|$ [where $\|\mathbf{x}\| \equiv (\Sigma_n x_n^2)^{1/2}$] falls below a preset threshold. The angular intensities are then summed over all directions and all collision orders in each cell to obtain the steady-state intensity. The sum over collisions of the light that is scattered out of the medium through each surface cell is taken as the steady-state detector reading R for a detector in the corresponding location on the surface of the medium. The detector readings are reported in units of photons emerging per incident photon per unit area.

The reference medium for which results presented below were computed was a homogeneous, nonabsorbing ($\mu_a = 0$) slab whose dimensions were $61 \times 61 \times 11$ cells. The scattering cross section was $\mu_s = 1$, i.e., one scattering per mfp. The scattering distribution was isotropic in all cells. The light source was modeled by specifying $\boldsymbol{\varphi} = 1$ in cell $(i, j, k) = (31, 31, 1)$, 0 elsewhere. Readings were computed for 62 distinct detectors, which were located on the exterior faces of cells $(i, 31, 1)$ and $(i, 31, 11)$, with $i = 1$–31.

To generate the one-absorber results presented here, the absorption cross section was perturbed in cell (31, 31, 5), (31, 30, 6), (31, 31, 6), (31, 31, 7), or (31, 31, 1). For each of the first four of these cells, we did calculations with $\Delta\mu_a = 0$, 0.05, 0.1, ..., 0.35, 0.4, 0.5, ..., 0.9, 1.0, and

∞. For a perturbation in cell (31, 31, 1), we used $\Delta\mu_a$ = 0, 0.02, ..., 0.22, 0.24, and 1.0.

In the two-absorber study whose results are shown below, the effects on detector readings of simultaneous absorption cross-section perturbations in cells (31, 31, 5) and (31, 31, 7) were computed. These computations employed the same sequence of values for the absorption probabilities as did the one-absorber studies. Internal collision rates and detector readings were obtained for every possible pairing of the $\Delta\mu_a$'s.

4.A.2. Analytic Solution to the Diffusion Equation

As a test of the accuracy of the relaxation solver, the diffuse transmittance and reflectance computed for the finite slab medium described above were compared to the corresponding fluxes computed from an analytic solution to the diffusion equation for an infinite slab. Let the diffusing medium be a homogeneous, nonabsorbing, isotropically scattering infinite slab with plane boundaries at $z = 0$ and $z = Z$ (all distances are in units of mean free paths). For such a slab, with a unit strength point source located at $(x, y, z) = (0, 0, z_s)$ and with extrapolated boundaries lying a distance z_0 outside the physical boundaries, the magnitude of the reflected flux at radial distance x from the source is

$$|\mathbf{J}(x, 0, 0)| = \frac{1}{4\pi}\left|\sum_{i=-\infty}^{\infty}\left[\alpha_i(x^2 + \alpha_i^2)^{-3/2} - \beta_i(x^2 + \beta_i^2)^{-3/2}\right]\right|, \qquad (4.A.1)$$

where $\alpha_i = 2iZ - z_s + (4i - 2)z_0$ and $\beta_i = 2iZ + z_s + 4iz_0$. For the same medium, the magnitude of the transmitted flux, $|\mathbf{J}(x, 0, Z)|$, is obtained by replacing α_i and β_i in Eq. (4.A.1) with, respectively, $\alpha_i - Z$ and $\beta_i - Z$.

The flux magnitudes $|\mathbf{J}(x, 0, 0)|$ and $|\mathbf{J}(x, 0, Z)|$ were calculated for many source depths $z_{s,i} = 0.1i$, i = 1–109, and at x = 0, 0.1, 0.2, 0.3, 0.4, 0.5, 1.0, 1.5, ..., 30.0, 30.5, with $z_0 = 0$ and again with $z_0 = 0.7104$. Each calculation was terminated when the ratio of the nth partial sum to the $(n - 1)$th differed from unity by less than 10^{-6} in absolute value.[17] The flux magnitudes corresponding to an exponentially attenuated line source were estimated by multiplying the flux arising from the ith point source by $e^{-z_{s,i}}/\Sigma_j e^{-z_{s,j}}$ and then summing over i. This procedure generates an approximate value for the flux across a boundary at a point; the point-flux estimates were numerically integrated using Simpson's rule to obtain estimates of fluxes through 1-mfp^2 surface area patches for comparison to the relaxation data.

4.A.3. Computation of Best-Fitting Parameter Values

All computations of best-fitting parameters referred to below were performed by using the nonlinear curve-fitting procedure of PSI-Plot version 4.51 for Windows. This uses a Marquardt–Levenburg algorithm[18] with a least-squares convergence criterion. For nonlinear model functions, the coefficient of determination (COD), which is the fraction of total variance in the data that is accounted for by the model,[19] was used to measure the goodness of fit.

4.B. Results

4.B.1. Accuracy of Numerical Flux Computations for a Homogeneous Medium

A sketch of the reference medium with its dimensions and the locations of the source and detectors explicitly indicated is shown in Fig. 1(b). One-dimensional detector arrays were specified on the slab's top and bottom faces in generating the computational results presented here; the lines along which the sets of reflectance detectors and transmittance detectors lay were all in the central plane $y = 31$. The computed fluxes of light reflected (open circles) and transmitted (open squares) across these two surfaces, as a function of the distance between the x coordinates of source and detector, are shown in Fig. 1(b). Shown on the same plot are two sets of curves obtained from the analytic solution of the diffusion equation for an infinite, 11-mfp-thick, nonabsorbing, homogeneous slab. These results were obtained with z_0 set to zero (solid

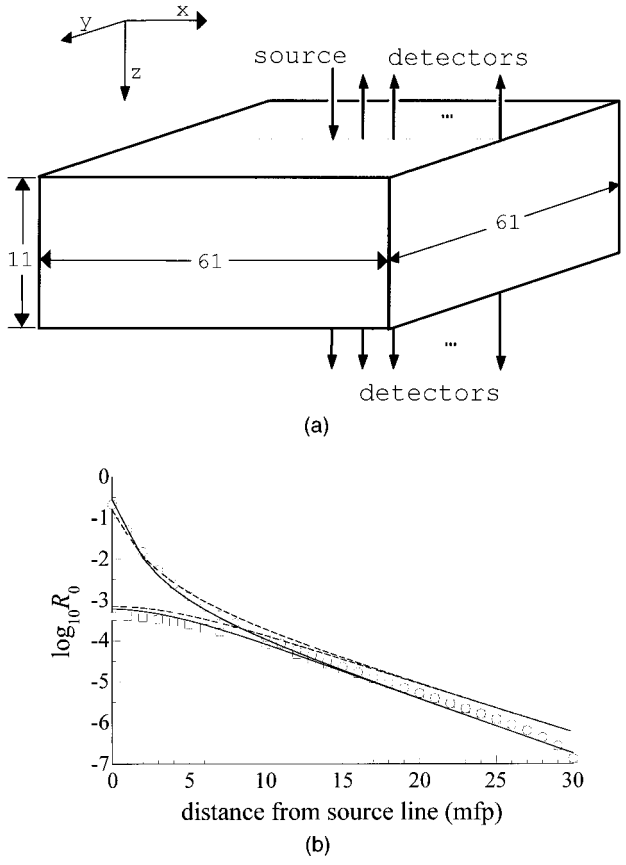

Fig. 1. Detector readings, homogeneous reference medium. (a) Sketch of three-dimensional homogeneous, isotropically scattering medium modeled in computation of reference detector readings by the relaxation code. Units of the indicated dimensions are numbers of cells. Also shown are source and detector locations; the two detector arrays are in the same plane. (b) Plot of base-ten logarithms of the computed detector readings for reflected (circles) and transmitted (squares) light, as a function of distance along the surface between the incident beam and the detector. Plotted curves are analytic diffusion equation solutions for an infinite homogeneous, nonabsorbing, isotropically scattering slab that is 11 mfp thick, with the diffuse intensity going to zero at the physical boundaries (solid curves) or at extrapolated boundaries 0.7104 mfp outside the physical boundaries (dashed curves).

curves) and to 0.7104 mfp (dashed curves). The good agreement between the numerical and analytic results indicates that the relaxation code computes an accurate numerical solution to the diffusion equation for this medium.

4.B.2. ΔR versus $\Delta\mu_a$, One Absorption Perturbation

Results of a one-absorber computation with $\Delta\mu_a$ located in cell (31, 31, 5) are shown for 4 of the 62 detectors in Fig. 2. Figure 2(a) is a sketch of the two-dimensional (2-D) section $y = 31$ of the slab, with the locations of the perturbed cell and the detectors indicated; the distance units are numbers of cells, and each cell's linear dimension is one mfp in the unperturbed reference medium. The absolute values of ΔR (i.e., $R_0 - R$, where R_0 is the reference medium detector reading) are plotted against $\Delta\mu_a$ in Fig. 2(b). Here (and in subsequent figures) $\Delta\mu_a$ is expressed as the percent increase in the perturbed cell's μ_t that is caused by the absorption perturbation. The data points for detectors `r2` (open circles) and `t2` (open triangles) appear to lie on the $\Delta\mu_a$ axis because the ΔR values for these detectors are 2–3 orders of magnitude smaller than are those for detectors `r1` (filled circles) and `t1` (filled triangles). The best fit of each set of data points to the equation

$$\Delta R = \frac{\Delta R^{\infty}\Delta\mu_a}{K + \Delta\mu_a} \qquad (4.B.1)$$

was computed using only the data for $\Delta\mu_a \leqslant 1.0$; the form of Eq. (4.B.1) follows directly from Eq. (3.C.4). The resulting best fits are plotted as solid curves through the data points, and the best-fitting parameters are given in Table 2; in every case the COD differed from unity by less than 10^{-8}.

Equation (4.B.1) is formally identical to the Michaelis–Menten equation of enzymology, which relates the rate of an enzyme-catalyzed reaction V to the concentration of substrate S. The ΔR^{∞} and K parameters are respectively analogous to $V_{\max}$ and K_{M}.

4.B.3. $\Delta R/\Delta R^{\infty}$ versus $\Delta\mu_a$, One Absorption Perturbation

In Table 2 it is seen that the values obtained for K are nearly identical for all four detectors indicated in Fig. 2(a), a result that lends computational validity to Eq. (3.C.8). Also, for each detector the ΔR^{∞} obtained from the curve fit is nearly identical to that computed by the relaxation solver when $\Delta\mu_a = \infty$. In Fig. 2(c) the data points and curves in Fig. 2(b) are replotted as $\Delta R/\Delta R^{\infty}$ vs. $\Delta\mu_a$. Each data point was normalized by dividing by the ΔR^{∞} obtained from the relaxation computation for the corresponding detector, and each curve by dividing by the ΔR^{∞} determined from the corresponding curve fit. As predicted by Eq. (3.C.8), the relation between $\Delta R/\Delta R^{\infty}$ and $\Delta\mu_a$ is independent of detector location; the distances between curves in Fig. 2(c) is less than the line thickness.

4.B.4. Dependence of Detector Readings on Perturbed Cell Location

Results of a study of the sensitivity of the parameter K in Eq. (4.B.1) to the location of the perturbed cell are shown in Fig. 3. Figure 3(a) is a sketch of the 2-D section $y = 31$ of the slab, with three locations [(31, 31, 1), (31, 31, 5), (31, 31, 7)] of the perturbed cell for which one-absorber computations were performed indicated. For each of these sites, the ratio $\Delta R(\Delta\mu_a)/\Delta R^{\infty}$ was calculated for every 1 of the 62 detectors and every value of $\Delta\mu_a$; for the case of $\Delta\mu_a \neq 0$ in cell (31, 31, 1), which blocks the source, each detector's ΔR^{∞} is equal to its R_0. Then the mean and standard deviation of $\Delta R(\Delta\mu_a)/\Delta R^{\infty}$ over the full set of detectors were calculated for each value of $\Delta\mu_a$. In Fig. 3(b), the mean values of

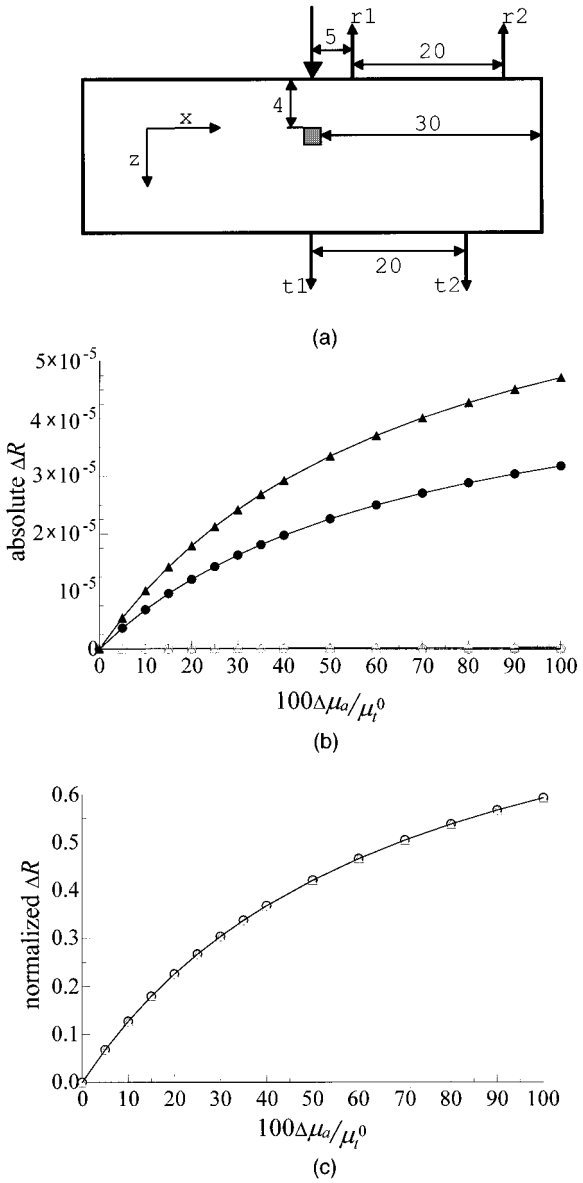

Fig. 2. Effect of a single localized $\Delta\mu_a$ on computed detector readings. (a) Sketch of 2-D section through the slab medium, showing the location of the perturbed cell [cell (31, 31, 5)] and four detectors. Units of indicated distances are numbers of cells. (b) ΔR vs. $\Delta\mu_a$ (in units of percent increase in the perturbed voxel's μ_t owing to the increased absorption), for the four detectors indicated in (a). Curves are best fits of Eq. (4.B.1) to the data points, using only the data points for finite values of μ_a. Data point–detector correspondences are as follows: filled circles, detector `r1`; filled triangles, detector `t1`; open circles, detector `r2`; open triangles, detector `t2`. (c) $\Delta R/\Delta R^{\infty}$ versus $\Delta\mu_a$ for the same detectors as in (b); symbols also are the same as in (b).

Table 2. Coefficients of Best Fits of Eq. (4.B.1) to the Four Sets of Data Points Shown in Fig. 2(b). Shown Also Are the Detector Readings' Perturbations Obtained from the Relaxation Computation When a Perfect Absorber Was Placed in the Cell Shaded in Fig. 2(a)

Detector Located over Cell	K	ΔR^{∞} from Curve Fit	ΔR^{∞} from Relaxation Computation
(26, 31, 1)	$0.68552 \pm 2 \times 10^{-5}$	$5.3684 \times 10^{-5} \pm 9 \times 10^{-10}$	5.3685×10^{-5}
(6, 31, 1)	$0.68550 \pm 1 \times 10^{-5}$	$1.2498 \times 10^{-7} \pm 1 \times 10^{-12}$	1.2498×10^{-7}
(31, 31, 11)	$0.685540 \pm 2 \times 10^{-6}$	$7.9602 \times 10^{-5} \pm 1 \times 10^{-10}$	7.9602×10^{-5}
(11, 31, 11)	$0.685545 \pm 1 \times 10^{-6}$	$5.2639 \times 10^{-7} \pm 6 \times 10^{-13}$	5.2639×10^{-7}

$\Delta R(\Delta\mu_a)/\Delta R^{\infty}$ are plotted against $\Delta\mu_a$ for each of the three cells indicated in Fig. 3(a). The associated standard deviations are shown in a base-ten, log-linear plot in Fig. 3(c). The greatest coefficient of variation for any single data point is 0.21%, when $\Delta\mu_a = 0.1$ in cell (31, 31, 7). For most data points, the coefficient of variation is less than 0.1%.

The curves sketched in Fig. 3(b) are plots of the best fits of the data points to the two-parameter model

$$\left\langle \frac{\Delta R}{\Delta R^{\infty}} \right\rangle = \lambda \frac{\Delta\mu_a}{K + \Delta\mu_a}. \tag{4.B.2}$$

The distance between the curves for $\Delta\mu_a$ in cell (31, 31, 5) (circles) and in cell (31, 31, 7) (squares) is less than the curve thickness. For $\Delta\mu_a$ in cell (31, 31, 1), the best fit to the model was calculated from only the data points for which $\Delta\mu_a \leq 0.24$, and the data point for $\Delta\mu_a = 1.0$ was computed afterward. The numerical values obtained for the best-fitting parameters, for the three cells indicated in Fig. 3(a) and for two other cells [(31, 31, 6), (31, 30, 6)], are given in Table 3; in all cases the COD differed from unity by less than 10^{-8}. Ideally, λ would be exactly 1.0 in all cases. The calculated λ differs from 1.0 by at most 0.0002; this maximum deviation was obtained for the set of data points encompassing the smallest range of $\Delta\mu_a$ values. There was no appreciable change in K, the COD, or the model selection criterion[19] computed for $\Delta\mu_a \neq 0$ in any cell when a one-parameter model was used in place of Eq. (4.B.2).

4.B.5. ΔR versus $\Delta\mu_a$, Two Absorption Perturbations

Results of a two-absorber computation for two specific detectors, and $\Delta\mu_a \neq 0$ in cells (31, 31, 5) and (31, 31, 7), are shown in Figure 4. Figure 4(a) is a sketch of the 2-D section $y = 31$, with the locations of the perturbed cells and the detectors indicated. The absolute value of ΔR for detector r is plotted against $\Delta\mu_{a,5} \equiv \Delta\mu_{a,(31,31,5)}$ and $\Delta\mu_{a,7} \equiv \Delta\mu_{a,(31,31,7)}$ in Fig. 4(b). Let us call the function graphed in Fig. 4(b) ΔR_c (for "coupled"), and let ΔR_i (for "independent") be the sum of the detector reading perturbations produced by $\Delta\mu_{a,5}$ and $\Delta\mu_{a,7}$ each acting alone. The absolute mutual coupling between cells (31, 31, 5) and (31, 31, 7), $\Delta R_i - \Delta R_c$, is shown in Fig. 4(c). The same data are replotted in Fig. 4(d) as the relative percent mutual coupling, $100(1 - \Delta R_c/\Delta R_i)$. ΔR_c, $\Delta R_i - \Delta R_c$, and $100(1 - \Delta R_c/\Delta R_i)$ for detector t are graphed in Figs. 4(e)–4(g).

The surfaces plotted in Figs. 4(e)–4(g) are symmetric about the line $\Delta\mu_{a,5} = \Delta\mu_{a,7}$. This was expected, for two reasons. First, the perturbed cells are symmetric about the midplane of the slab and the reference medium is homogeneous, and therefore $(T_0)_{pp} = (T_0)_{qq}$ and both linear terms in the denominator of Eq. (3.D.6) should have the same coefficient. Second, the absorption weights [as de-

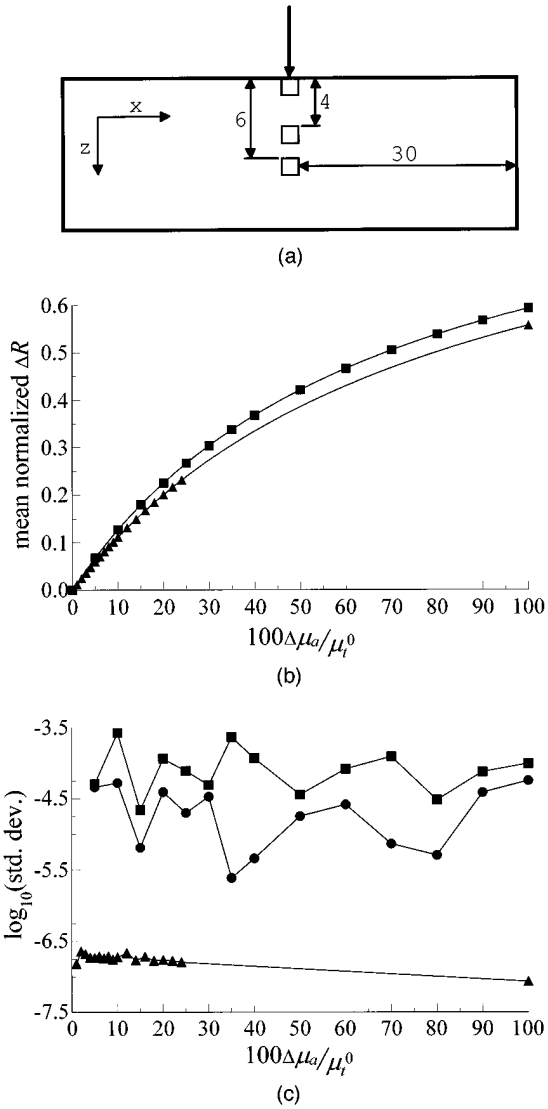

Fig. 3. Dependence of $\Delta R/\Delta R^{\infty}$ on location of a single $\Delta\mu_a$. (a) Sketch of 2-D section through the slab medium, showing three alternative locations for the perturbed cell [(31, 31, 1), (31, 31, 5), or (31, 31, 7)]. Units of indicated distances are numbers of cells. For each $\Delta\mu_a$ location and magnitude the ratio $\Delta R(\Delta\mu_a)/\Delta R^{\infty}$ was calculated for each of the 62 detectors, and the mean and standard deviation over the set of detectors were then computed. (b) Plots of $\overline{\Delta R(\Delta\mu_a)/\Delta R^{\infty}}$ versus $\Delta\mu_a$, for $\Delta\mu_a$ in each of the three cells indicated in (a). Data point–perturbed cell correspondences are as follows: circles, cell (31, 31, 5); squares, cell (31, 31, 7); triangles, cell (31, 31, 1). (c) Plots of $\log_{10}\{\sigma[\Delta R(\Delta\mu_a)/\Delta R^{\infty}]\}$ versus $\Delta\mu_a$. Units and symbols are the same as in (b).

Table 3. Coefficients of Best Fits of Eq. (4.B.2) to the Three Sets of Data Points Shown in Fig. 3(b) and for Two Other Locations of the Absorption Perturbation Not Shown in Fig. 3

Perturbed Cell	λ	K
(31, 31, 1)	$0.99979 \pm 6 \times 10^{-5}$	$0.79427 \pm 6 \times 10^{-5}$
(31, 31, 5)	$0.99998 \pm 2 \times 10^{-5}$	$0.68553 \pm 2 \times 10^{-5}$
(31, 31, 7)	$1.00001 \pm 5 \times 10^{-5}$	$0.68557 \pm 6 \times 10^{-5}$
(31, 31, 6)	$1.00001 \pm 2 \times 10^{-5}$	$0.68444 \pm 2 \times 10^{-5}$
(31, 30, 6)	$0.99999 \pm 2 \times 10^{-5}$	$0.68434 \pm 3 \times 10^{-5}$

fined in the text following Eq. (1.1)] of the two cells are equal for detector t because of the inline transmission geometry and the homogeneity of the reference medium, and therefore both linear terms in the numerator of Eq. (3.D.6) should have the same coefficient. The surface in Fig. 4(c) also is symmetric about $\Delta\mu_{a,5} = \Delta\mu_{a,7}$ within the domain of the plot; however, it would become more visibly asymmetric if the domain were extended to include values of $\Delta\mu_{a,5}$ and $\Delta\mu_{a,7}$ greater than unity.

The ΔR_c and ΔR_i data were fitted to the equations

$$\Delta R = \frac{a_n\Delta\mu_{a,5} + b_n\Delta\mu_{a,7} + c_n\Delta\mu_{a,5}\Delta\mu_{a,7}}{1 + a_d\Delta\mu_{a,5} + b_d\Delta\mu_{a,7} + c_d\Delta\mu_{a,5}\Delta\mu_{a,7}} \tag{4.B.3a}$$

for detector r, and

$$\Delta R = \frac{a_n(\Delta\mu_{a,5} + \Delta\mu_{a,7}) + c_n\Delta\mu_{a,5}\Delta\mu_{a,7}}{1 + a_d(\Delta\mu_{a,5} + \Delta\mu_{a,7}) + c_d\Delta\mu_{a,5}\Delta\mu_{a,7}} \tag{4.B.3b}$$

for detector t; these functional forms follow directly from Eqs. (3.D.6) and (3.D.7), and the four-parameter model is appropriate for detector t because of the symmetry of ΔR about $\Delta\mu_{a,5} = \Delta\mu_{a,7}$. The numerical values obtained for the best-fitting parameters are given in Table 4; in all cases the COD differed from unity by less than 10^{-8}. Equations (3.D.6) and (3.D.7) differ only in the coefficients of the quadratic terms, and this is also what we see in the calculations. For detector r, a_d and b_d are essentially equal. This was expected because the elements of $\mathbf{T}_0$ for the two perturbed cells are equal in the medium that we specified. There was no appreciable change in the best-fitting parameter values, the COD, or the model selection criterion when a five-parameter model that replaces b_d with a_d was used in place of Eq. (4.B.3a).

5. DISCUSSION

The current work was motivated by the prospect of obtaining a simple improvement to linear perturbation theory. We have derived expressions for the net ΔR caused by $\Delta\mu_a$'s of any magnitude in any one [Eq. (3.C.4)] or two [Eq. (3.D.6)] voxels. These can, in principle, be generalized to conditions of time harmonic illumination and anisotropic scattering.

Comparison of detector readings computed by the relaxation method to those obtained from analytic diffusion equation solutions shown in Fig. 1 (and comparisons, not shown, of intensities at locations in the slab interior) gives us confidence in the numerical data.

For a medium containing one μ_a perturbation, Eq. (3.C.4) shows that the condition for validity of the linear approximation, Eq. (1.1), is $z \ll 1/(\mathbf{T}_0)_{qq}$, where $z = \Delta\mu_{a,q}/\mu^0_{t,q}$ in the lattice case and $z = \Delta\mu_{a,q}\ell_q$ in the continuum case. From the results shown in Fig. 2 and Fig. 3, we see that for the particular reference medium and $\Delta\mu_a$ locations considered, all ΔRs are nearly proportional to $\Delta\mu_{a,q}$ when $\Delta\mu_{a,q} \leqslant 0.1\mu^0_{t,q}$, a finding which is consistent with the rule-of-thumb used by researchers computing transport equation solutions.[20] From Eq. (3.D.6) we can likewise obtain the conditions for validity of Eq. (1.1) in a medium containing two μ_a perturbations.

The one-perturbation results shown in Fig. 2 and Fig. 3 are fully consistent with the theoretical derivation in Subsection 3.C. Perturbations in individual detector readings depend on the magnitude of $\Delta\mu_a$ in the manner predicted by Eq. (3.C.4), and the quantity $\Delta R_i(\Delta\mu_{a,q})/\Delta R_i(\infty)$ exhibits no dependence on the detector location beyond that which numerical roundoff errors could be expected to cause [Fig. 2(c), Fig. 3(c), and Table 2]. In terms of the quantities in Eq. (3.C.4), the parameter K that appears in Eq. (4.B.1) is equal to $\mu^0_{t,q}/(\mathbf{T}_0)_{qq}$ (lattice case) or $1/[(\mathbf{T}_0)_{qq}\ell_q]$ (continuum case). $\mu^0_{t,q}$ is independent of q for the lattice media used in our numerical studies, so K is simply inversely proportional to $(\mathbf{T}_0)_{qq}$. We would expect $(\mathbf{T}_0)_{qq}$ to be smaller for a voxel/cell near a boundary than for a deep-lying one, because a photon colliding with a near-surface cell is more likely to exit the medium before it has another collision in the same cell. This is consistent with the results of the one-absorber studies, where the largest K was obtained when the perturbed cell is (31, 31, 1).

The two-absorber results shown in Fig. 4 are fully consistent with the equations derived in Subsection 3.D. Perturbations in individual detector readings depend on the magnitude of $\Delta\mu_{a,q}$ and $\Delta\mu_{a,p}$ in just the manner predicted by Eq. (3.D.6). In contrast to the one-perturbation case, the shape of the ΔR_i surface as a function of $\Delta\mu_{a,p}$ vs. $\Delta\mu_{a,q}$ depends upon the detector location.

In the relaxation model, photons travel in steps of exactly one mfp between successive collisions. Further, all incident photons experience their first collision in the first-layer cell directly beneath the source [i.e., even when $\Delta\mu_a$ is in cell (31, 31, 1), the spatial distribution of first collisions is unaffected], and all photons entering a given detector have their last collision in the first-layer cell directly beneath the detector. As a consequence the relaxation model satisfies the assumptions made. These properties would not be changed by replacing the isotropic scattering used to generate the results with forward-directed scattering. Again, these are features that are shared by any theory or computation that models light propagation as a random walk, or any other Markov process, with a fixed step size. In addition, any numerical method for solving the diffusion equation that replaces the second-order differential operator with a three-point nearest-neighbor formula is again of this form. Therefore, to the extent that either random-walk or diffusion theory is an adequate representation of light propagation

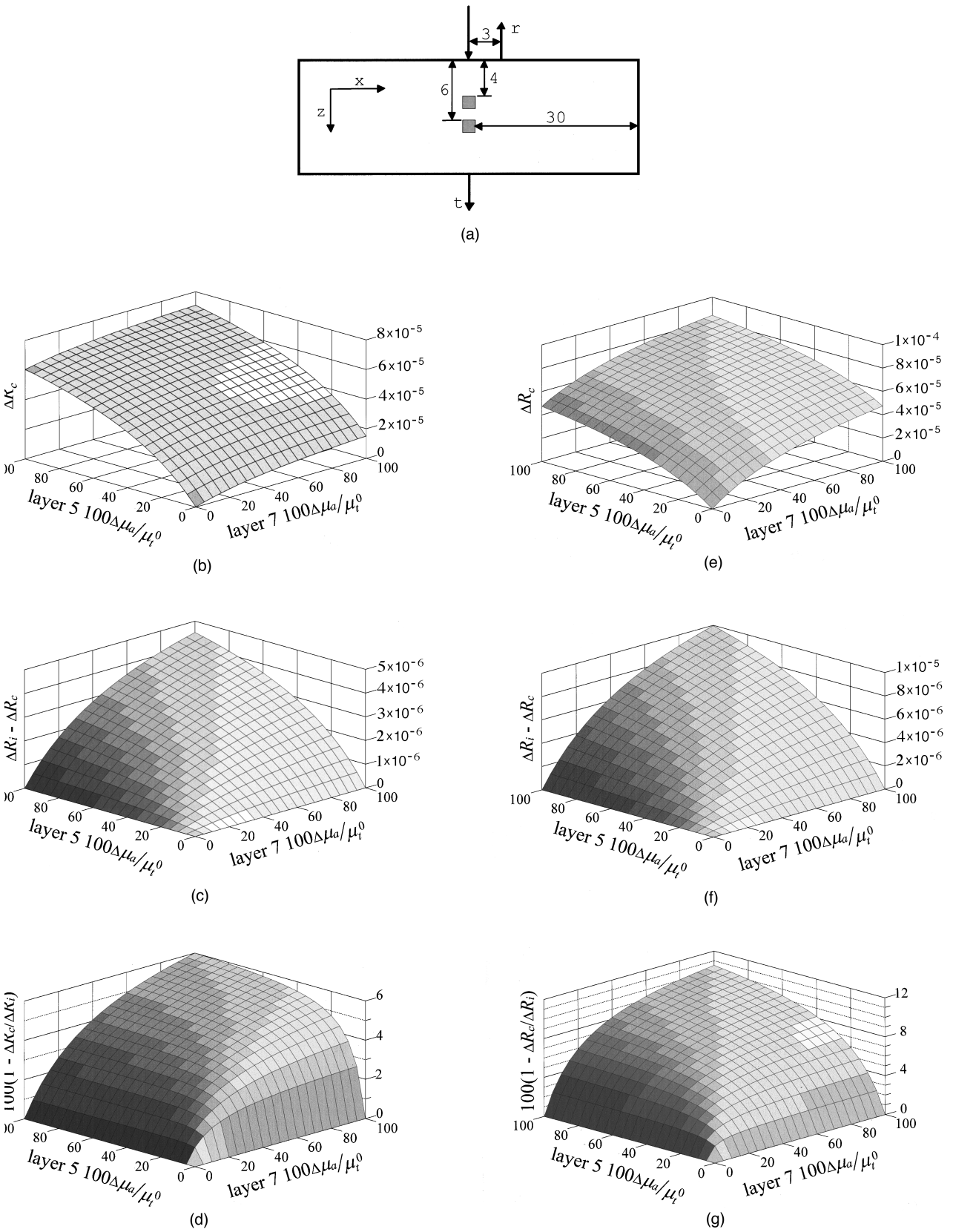

Fig. 4. Mutual coupling between two localized absorption perturbations. (a) Sketch of 2-D section through the slab medium, showing locations of the two perturbed cells [(31, 31, 5) and (31, 31, 7)] and two detectors. Units of indicated distances are numbers of cells. (b) Effect of two simultaneous localized $\Delta\mu_a$'s, ΔR_c vs. $\Delta\mu_{a,5}$ versus $\Delta\mu_{a,7}$, for detector r indicated in (a). (c) Absolute mutual coupling between the two cells indicated in (a), i.e., $\Delta R_c - \Delta R_i$. (d) Percent relative mutual coupling between the two cells indicated in (a), i.e., $100(1 - \Delta R_c/\Delta R_i)$, for detector r. (e)–(g) show the same quantities as in (b)–(d), but for detector t.

in a turbid medium, the assumptions of our theoretical model are satisfied.

5.A. Comparison with Findings of Other Investigators

The collision expansion is a well-known method for constructing formal solutions to transport problems.[21] Here we have used it as a means of deriving expressions for the net effect of one or two localized absorption perturbations on the photon intensity distribution in such a medium. It is important to note that the particular relation between **P** and **T** given by Eq. (2.A.2) is not exclusively a consequence of the physics of photon propagation. Rather, an analogous result is obtained for any phenomenon that can be modeled as a Markov process with absorbing states. Beltrami,[22] for example, has shown how a variety of problems in the biological and social sciences give rise to such processes. In every case a formulation having the same form as Eq. (2.A.2) is involved.

For example, a Markov model of photon propagation in which the photons migrate in uniform one-cell steps has been used by Grünbaum in his analysis of the turbid-medium inverse problem.[23] The expression he obtains for the input-output matrix Q_{IO} (i.e., the matrix of probabilities of going from any given source to any given detector) is $Q_{IO} = P_{IO} + P_{IH}(I - P_{HH})^{-1}P_{HO}$ [which has the same form as Eq. (3.A.1)], where the P's are one-step transition matrices and the indices I, O and H denote input, output and hidden, respectively. He describes the equivalent representation that the factor $(I - P_{HH})^{-1}$ has as an infinite series whose terms specify all possible pathways by which a medium can evolve from its first hidden state to its final one.

Several formal analyses of propagation of light through a scattering medium have resulted in rational-function formulations analogous to ours for the effect of one localized absorption perturbation. The various approaches taken do not, however, appear to be readily extendable to the case of two (or more) absorbers. For example, Furutsu and Yamada[14] analytically derive the effect that an isolated absorption perturbation has on solutions to the diffusion equation. They obtain an equation that is of the same form as Eq. (3.C.4) [Eq. (56) in Ref. 14] for a Fourier-space scattering matrix and that is a function of only the absorption perturbation and the diffusion-equation solution for the unperturbed medium.

A similar result is obtained by Gandjbakhche *et al.* in a different context.[15] They use random-walk theory to analyze the effect of a single localized absorption perturbation on transillumination measurements through an optically turbid slab. They derive an expression for the difference between the probabilities of a photon arriving at a given location after a set number of random-walk steps in the absence and presence of the absorber. Their formula contains a factor with a rational-function form similar to that of Eq. (3.C.8), especially for optically thick slabs.

Expressions similar to those derived here also have been arrived at previously through independent means. An example is the work of Howard *et al.* on the problem of reconstructing the apparent conductivity of inhomogeneous layered media based on measurements of induced voltage.[24] They seek to compute $\Delta\sigma(x')$, the difference between the inhomogeneous conductivity and a constant background conductivity, and show that the error caused by making the Born approximation can be corrected by replacing $\Delta\sigma(x')$ with $\Delta\sigma(x')/[1 - \alpha\Delta\sigma(x')]$ in their integral equation, where α is an empirically determined constant. The nonlinear effect of each heterogeneity upon itself is thus accounted for, but again it is not clear that the method can be extended to accounting for the effects of two heterogeneities on each other.

5.B. Computation of $\mathbf{P}_0$ and $(\mathbf{I} - \mathbf{P}_0)^{-1}$

In this work it was not actually necessary to compute $\mathbf{P}_0$ or $\mathbf{T}_0$ for any medium. We used these matrices only as stepping stones in the derivations of Eqs. (3.C.4) and (3.D.6). The significance of these equations lies in their functional forms, and their utility does not require an ability to evaluate the expressions for the coefficients in terms of elements of $\mathbf{T}_0$ and $\mathbf{r}_0$. As shown below in Subsection 5.D, these coefficients have alternative expressions in terms of quantities that can be computed by other means.

It is interesting nevertheless to address the question of whether $\mathbf{P}_0$ and $\mathbf{T}_0$ could be explicitly computed in an ef-

Table 4. Coefficients Obtained by Fitting the Coupled ΔR and Independent ΔR for Detectors r and t [See Fig. 4(a)] to Eqs. (4.B.3a) and (4.B.3b), Respectively

Coefficient	Detector r, Coupled	Detector r, Independent	Detector t, Coupled	Detector t, Independent
a_n	1.484979×10^{-4} $\pm 7 \times 10^{-10}$	1.484971×10^{-4} $\pm 9 \times 10^{-10}$	1.161159×10^{-4} $\pm 5 \times 10^{-10}$	1.161166×10^{-4} $\pm 4 \times 10^{-10}$
b_n	3.70941×10^{-5} $\pm 6 \times 10^{-10}$	3.70914×10^{-5} $\pm 6 \times 10^{-10}$	$= a_n$	$= a_n$
c_n	2.40447×10^{-4} $\pm 7 \times 10^{-9}$	2.70710×10^{-4} $\pm 8 \times 10^{-9}$	2.75103×10^{-4} $\pm 4 \times 10^{-9}$	3.38746×10^{-4} $\pm 3 \times 10^{-9}$
a_d	1.45868 $\pm 1 \times 10^{-5}$	1.45868 $\pm 2 \times 10^{-5}$	1.45871 $\pm 1 \times 10^{-5}$	1.45873 $\pm 1 \times 10^{-5}$
b_d	1.45870 $\pm 4 \times 10^{-5}$	1.45855 $\pm 4 \times 10^{-5}$	$= a_d$	$= a_d$
c_d	2.08686 $\pm 7 \times 10^{-5}$	2.12772 $\pm 7 \times 10^{-5}$	2.08681 $\pm 5 \times 10^{-5}$	2.12767 $\pm 4 \times 10^{-5}$

ficient manner. Imaging problems of practical interest can be expected to involve 10^4 to 10^6 voxels or even more. This is the same as the number of columns of $\mathbf{P}_0$, each one of which requires a separate computation in the general case of a heterogeneous medium. Thus it appears that $\mathbf{P}_0$ could not be computed in practice in an acceptably brief time. However, the problem may be more tractable than this in reality, because only the first collision of each photon is relevant. Certainly it is easy to compute $\mathbf{P}_0$ for a homogeneous medium, and in any case computation of $\mathbf{P}_0$ does not require solution of a transport (or diffusion) equation.

Accurate computation of $\mathbf{T}_0$ might well be accomplished at reasonable cost by inverting $\mathbf{I} - \mathbf{P}_0$, in spite of the large size of $\mathbf{P}_0$. It should be possible to replace many very small elements of $\mathbf{P}_0$ with zeroes, resulting in a sparse matrix. Thus computation of $\mathbf{T}_0 = (\mathbf{I} - \mathbf{P}_0)^{-1}$ from $\mathbf{P}_0$ is a well-conditioned inverse problem, and one to which efficient specialized algorithms developed for sparse matrices are applicable. In the case of a homogeneous medium we would also make use of the fact that in all regions far from a boundary, any two elements of $\mathbf{T}_0$ with the same intervoxel spacing would be about the same.

5.C. Higher-Order Corrections

It may be obvious to some that the method of Subsections 3.C and 3.D can be extended to the case of n absorbers by including a total of n nonzero elements in $\mathbf{Y}$ when evaluating Eqs. (3.B.10) and (3.B.11). The magnitudes of successive corrections typically will decrease steadily with increasing n, and this militates against undertaking the effort of computing higher-order interaction formulas for two reasons. First, the algebraic labor involved increases with increasing n. Second, as n grows the errors arising from the assumptions introduced in Subsection 3.B eventually will be greater than the corrections.

5.D. Possible Applications to Image Reconstruction

There have been published reports on algorithms for image reconstruction that recognized that Eq. (1.1) does not accurately express the dependence of ΔR_i on $\Delta\boldsymbol{\mu}_a = [\Delta\mu_{a,1}\Delta\mu_{a,2}\ldots\Delta\mu_{a,I}]^T$. These have suggested that a Newton-type updating scheme be adopted for image reconstruction, that is, that the forward and inverse problems be solved repeatedly in an alternating sequence.[7,9,25] The nth computed solution to the inverse problem would be used to modify the properties of the reference medium, e.g., $\mu^0_{a,i}(n) = \mu^0_{a,i}(n-1) + \Delta\mu_{a,i}(n)$, then the weight functions and reference detector readings would be recomputed for the revised reference medium, and these would then be used to compute the $(n+1)$th inverse problem solution.

Newton update computations can be lengthy and difficult. The formulas in Subsections 3.C and 3.D suggest an attractive alternative. There are two principal questions that must be addressed. First, how may precise numerical values of the coefficients multiplying the assorted terms in Eqs. (3.C.4) and (3.D.6) be determined? Second, exactly how may we make use of the equations in an image reconstruction algorithm once the numerical values of the coefficients are known?

5.D.1. Quantitative Evaluation of Coefficients in Eqs. (3.C.4) and (3.D.6)

We proceed from the premise that the elements of $\mathbf{T}_0$ will not be directly computed. Two practical approaches for evaluation of the coefficients in Eq. (3.C.4) have been identified. The second of these can also be used to evaluate the coefficients in Eq. (3.D.6).

In the first approach (an equivalent form of this was presented earlier[10]), we begin by taking the low-absorption limit of Eq. (4.B.1), $\lim_{\Delta\mu_{a,j}\to 0}\Delta R^j_i = \Delta R^{\infty j}_i\Delta\mu_{a,j}/K$, and identify the coefficient of $\Delta\mu_{a,i}$ with the weight function w_{ij}. Then Eq. (4.B.1) becomes

$$\Delta R^j_i = \frac{w_{ij}\Delta R^{\infty j}_i\Delta\mu_{a,j}}{\Delta R^{\infty j}_i + w_{ij}\Delta\mu_{a,j}}. \tag{5.D.1}$$

Methods for calculating w_{ij} in terms of forward-problem solutions for the reference medium are well known. To determine numerical values for $\Delta R^{\infty j}_i$ it is necessary to perform additional forward-problem computations with $\mu_{a,j} = \infty$ in voxel j. This would be an impractical procedure if it were necessary to perform a separate computation for every combination of i and j, but there are at least three reasons why this might not be necessary in practice. First, for a fixed j, the $\Delta R^{\infty j}$s for any two detectors i and i' are related by $\Delta R^{\infty j}_{i'} = \Delta R^{\infty j}_i(w_{i'j}/w_{ij})$, so once $\Delta R^{\infty j}_i$ is computed for any one detector it is computed for all detectors. Second, in the important special case in which j is a voxel at the medium's surface, a detector can always be placed directly over it. There is no need to compute $\Delta R^{\infty j}$ for this detector; $\Delta R^{\infty j}_i = R_{0,i}$, and the $\Delta R^{\infty j}$s for all other detectors are then determined just as in the previous case. Third, results so far obtained suggest that $\Delta R^{\infty j}_i$ may in practice be a slowly varying function of the perturbed voxel's location (although more results computed for heterogeneous media are necessary to support or refute this), in which case it could be sufficient to divide the reference medium into a number of regions much smaller than the total number of voxels, and perform a single forward-problem computation for each of them.

This method does not generalize to a practical procedure for evaluating the coefficients in Eq. (3.D.6). In order to evaluate the coefficients multiplying $\Delta\mu_{aj}\Delta\mu_{aj'}$, it would be necessary to compute forward-problem solutions for two additional combinations of $\Delta\mu_{aj}$ and $\Delta\mu_{aj'}$, for (in principle) every possible j,j' pairing of voxels in the medium. That is, as many as $I(I-1)$ additional forward computations would be needed for a medium with I voxels. Although the number required in practice ordinarily would be smaller than this because mutual coupling typically becomes negligible for voxels separated by more than a few mean free paths, we would still expect that it would be impractically large.

The second approach involves computation of the coefficients of Eq. (3.C.4) from first principles. Let ϕ^{+0}_{ij} be the adjoint Green's function for the background medium: the volume-integrated intensity in voxel i due to one photon born per second in voxel j, or, equivalently, the volume-integrated fluence in i due to one photon born in j. Suppose that the intensity in voxel j is ϕ^0_j. Then

$\mu_{t,j}^0\phi_j^0$ is the collision density in voxel j, and so $\phi_{ij}^{+0}V_j\mu_{t,j}^0\phi_j^0$ is the volume-integrated intensity in i due to intensity ϕ_j^0, where V_j is the volume of voxel j. By our definition of $\mathbf{T}_0$, this is just $V_j(\mathbf{T}_0)_{ij}\phi_j^0$. Since this relation is an identity, for any ϕ_j^0 it follows that

$$(\mathbf{T}_0)_{ij} = \mu_{t,j}^0\phi_{ij}^{+0} \tag{5.D.2}$$

and therefore that

$$\begin{aligned}\Delta R_i^j &= \frac{\left[\phi_j^0\sum_{k=1}^{I} r_{0,i,k}(\mathbf{T}_0)_{kj}\right]\Delta\mu_{a,j}}{\kappa_j + (\mathbf{T}_0)_{jj}\Delta\mu_{a,j}} \\ &= \frac{\left(\phi_j^0\sum_{k=1}^{I} r_{0,i,k}\mu_{t,k}^0\phi_{kj}^{+0}\right)\Delta\mu_{a,j}}{\kappa_j + (\mu_{t,j}^0\phi_{jj}^{+0})\Delta\mu_{a,j}} \\ &= \frac{\left(\sum_{k=1}^{I} r_{0,i,k}\mu_{t,k}^0 w_{kj}\right)\Delta\mu_{a,j}}{\kappa_j + (\mu_{t,j}^0\phi_{jj}^{+0})\Delta\mu_{a,j}},\end{aligned} \tag{5.D.3}$$

where $r_{0,i,k}$ denotes the kth component of the ith detector response function. In Eq. (5.D.3) we use the familiar definition of absorption weight as the product of an intensity and an adjoint, $w_{ij} = \phi_j^0\phi_{ij}^{+0}$. This is the correct definition for the absorption weight under the constraint that the transport cross section (or, equivalently, the diffusion coefficient) is fixed. It would be necessary to perform forward-problem computations of ϕ_{kj}^{+0} for computation of the intervoxel weight functions.

The same idea can be adapted to the problem of evaluating the coefficients in Eq. (3.D.6). Application of Eq. (5.D.2) gives us

$$\Delta R_i^{jj'} = \frac{\sum_{k=1}^{I} r_{0,i,k}\{w_{kj}z' + w_{kj'}\nu' + A_{j,j',k}z'\nu'\}}{1 + \phi_{jj}^{+0}z' + \phi_{j'j'}^{+0}\nu' + B_{j,j'}z'\nu'}, \tag{5.D.4}$$

for the perturbation of the ith detector reading caused by $\Delta\mu_a \neq 0$ in voxels j and j', where $A_{j,j',k} \equiv w_{kj}\phi_{j'j'}^{+0} + w_{kj'}\phi_{jj}^{+0} - w_{jj'}\phi_{kj}^{+0} - w_{j'j}\phi_{kj'}^{+0}$, $B_{j,j'} \equiv \phi_{jj}^{+0}\phi_{j'j'}^{+0} - \phi_{j'j}^{+0}\phi_{jj'}^{+0}$, $z' = \mu_{t,j}^0 z$ and $\nu' = \mu_{t,j'}^0\nu$. Note that in the lattice case the variables z' and ν' are respectively equal to the absolute absorption perturbations $\Delta\mu_{a,j}$ and $\Delta\mu_{a,j'}$. The mutual coupling effect lies in the terms containing $\phi_{jj'}^{+0}$, $\phi_{j'j}^{+0}$, $w_{jj'}$ or $w_{j'j}$.

We stress that the intervoxel adjoints and weights in these formulas are for the reference medium, so that they can be precomputed and a library of values built up.

5.D.2. Incorporation of Corrections into Image-Reconstruction Algorithms

Here we assume the numerical values of all coefficients in Eq. (5.D.3) and Eq. (5.D.4) are known and address the practical problem of inverting them. We begin by considering only the single-absorber effect, in which case Eq. (1.1) is replaced by

$$\begin{aligned}\Delta R_i &= \sum_{j=1}^{I}\frac{w_{ij}\Delta\mu_{a,j}}{1 + \kappa_j\Delta\mu_{a,j}} \\ &= \sum_{j=1}^{I}\left(\frac{w_{ij}}{1 + \kappa_j\Delta\mu_{a,j}}\right)\Delta\mu_{a,j} \\ &\equiv \sum_{j=1}^{I} w'_{ij}\Delta\mu_{a,j}\end{aligned} \tag{5.D.5}$$

in order to correctly represent the dependence of ΔR_i on $\Delta\boldsymbol{\mu}_a$. Then $\Delta\boldsymbol{\mu}_a$ can in principle be found by solving the linear system $\Delta\mathbf{R} = \mathbf{W}'\Delta\boldsymbol{\mu}_a$. However, calculation of the correct numerical value for w'_{ij} requires knowledge of the unknown $\Delta\mu_{a,j}$. It should be possible to approach the correct $\Delta\boldsymbol{\mu}_a$ as the limiting value of a two-stage iterative process: solve the linear system $\Delta\mathbf{R} = \mathbf{W}'(n-1)\Delta\boldsymbol{\mu}_a(n)$ [with $\mathbf{W}'(0) = \mathbf{W}$], and substitute $\Delta\mu_{a,j}(n)$ into the expression for w'_{ij} to compute $w'_{ij}(n)$, etc.

When the two-absorber effect also is taken into account, the dependence of ΔR_i on $\Delta\boldsymbol{\mu}_a$ becomes

$$\Delta R_i = \sum_{j=1}^{I} w'_{ij}\Delta\mu_{a,j} - \frac{1}{I-1}\sum_{j=1}^{I-1}\sum_{j'=j+1}^{I}\frac{P_i(\Delta\mu_{a,j},\,\Delta\mu_{a,j'})}{Q_i(\Delta\mu_{a,j},\,\Delta\mu_{a,j'})}, \tag{5.D.6}$$

where $P_i(\Delta\mu_{a,j},\,\Delta\mu_{a,j'})/Q_i(\Delta\mu_{a,j},\,\Delta\mu_{a,j'})$ is the rational function (Table 1) for the effect of mutual coupling between voxels j and j' on detector i. Let us denote the second term on the right-hand side of Eq. (5.D.6) by b_i. Then $\Delta\boldsymbol{\mu}_a$ can in principle be found by solving the linear system $(\Delta\mathbf{R})' \equiv \Delta\mathbf{R} + \mathbf{b} = \mathbf{W}'\Delta\boldsymbol{\mu}_a$. The vector $\mathbf{b}$, like $\mathbf{W}'$, cannot be calculated without knowledge of $\Delta\boldsymbol{\mu}_a$. Successive estimates of $\mathbf{b}$ could, however, be computed in an iterative approach analogous to the one outlined above. Many variants are possible. At one extreme, $\mathbf{b}(n)$ can be computed within each iteration of the algorithm used to calculate the solution of $[\Delta\mathbf{R}(n)]' = \mathbf{W}'(n)\Delta\boldsymbol{\mu}_a(n)$. At the other, the system $\Delta\mathbf{R} = \mathbf{W}'(n)\Delta\boldsymbol{\mu}_a(n)$ can be solved before the first estimate, $\mathbf{b}(1)$, of $\mathbf{b}$ is computed, then the system $[\Delta\mathbf{R}(1)]' = \mathbf{W}'(n)\Delta\boldsymbol{\mu}_a(n)$, etc.

6. ACKNOWLEDGMENTS

This work was supported in part by the National Institutes of Health under grants RO1-CA59955 and RO1-CA66184, by the U.S. Office of Naval Research under grant N000149510063, and by the New York State Science and Technology Foundation. H. L. Graber acknowledges N. J. McCormick and R. E. Alcouffe for helpful discussions regarding, respectively, the theoretical model presented here and the numerical data used to test its

predictions. Thanks are due also to P. C. Koo for providing us the code used to generate the data presented in Section 4.

Correspondence should be addressed to R. L. Barbour, SUNY Health Science Center at Brooklyn, Box 25, 450 Clarkson Avenue, Brooklyn, New York 11203; tel: 718-270-1284; fax: 718-270-1305.

REFERENCES AND NOTES

1. R. L. Barbour, H. L. Graber, J. Chang, S.-L. S. Barbour, P. C. Koo, and R. Aronson, "MRI-guided optical tomography: prospects and computation for a new imaging method," IEEE Computational Sci. Eng. **2**, 63–77 (1995).
2. J. Chang, H. L. Graber, R. L. Barbour, and R. Aronson, "Recovery of optical cross-section perturbations in dense-scattering media using transport-theory-based imaging operators and steady-state simulated data," Appl. Opt. **35**, 3963–3978 (1996).
3. Y. Yao, Y. Wang, Y. Pei, W. Zhu, and R. L. Barbour, "Frequency-domain optical imaging of absorption and scattering distributions by a Born iterative method," J. Opt. Soc. Am. A **14**, 325–342 (1997).
4. R. L. Barbour, H. L. Graber, Y. Wang, J. Chang, and R. Aronson, "A perturbation approach for optical diffusion tomography using continuous-wave and time-resolved data," in *Medical Optical Tomography: Functional Imaging and Monitoring*, G. Müller, B. Chance, R. Alfano, S. Arridge, J. Beuthan, E. Gratton, M. Kaschke, B. Masters, S. Svanberg, and P. van der Zee, eds., Vol. IS11 of SPIE Institutes for Advanced Optical Technologies (SPIE Press, Bellingham, Wash., 1993), pp. 87–120.
5. H. L. Graber, J. Chang, R. Aronson, and R. L. Barbour, "A perturbation model for imaging in dense scattering media: derivation and evaluation of imaging operators," in *Medical Optical Tomography: Functional Imaging and Monitoring*, G. Müller, B. Chance, R. Alfano, S. Arridge, J. Beuthan, E. Gratton, M. Kaschke, B. Masters, S. Svanberg, and P. van der Zee, eds., Vol. IS11 of SPIE Institutes for Advanced Optical Technologies (SPIE Press, Bellingham, Wash., 1993), pp. 121–143.
6. S. R. Arridge, "The forward and inverse problems in time resolved infra-red imaging," in *Medical Optical Tomography: Functional Imaging and Monitoring*, G. Müller, B. Chance, R. Alfano, S. Arridge, J. Beuthan, E. Gratton, M. Kaschke, B. Masters, S. Svanberg, and P. van der Zee, eds., Vol. IS11 of SPIE Institutes for Advanced Optical Technologies (SPIE Press, Bellingham, Wash., 1993), pp. 35–65.
7. H. Jiang, K. D. Paulsen, U. L. Osterberg, B. W. Pogue, and M. S. Patterson, "Optical image reconstruction using frequency-domain data: simulations and experiments," J. Opt. Soc. Am. A **13**, 253–266 (1996).
8. M. A. O'Leary, D. A. Boas, B. Chance, and A. G. Yodh, "Images of inhomogeneous turbid media using diffuse photon density waves," in *OSA Proceedings on Advances in Optical Imaging and Photon Migration*, R. R. Alfano, ed., Vol. 21 of OSA Proceedings Series (Optical Society of America, Washington, D.C., 1994), pp. 106–115.
9. W. C. Chew and Y. M. Wang, "Reconstruction of two-dimensional permittivity distributions using the distorted Born iterative method," IEEE Trans. Med. Imaging **9**, 218–225 (1990).
10. H. L. Graber, R. L. Barbour, J. Chang, and R. Aronson, "Identification of the functional form of nonlinear effects of localized finite absorption in a diffusing medium," in *Proceedings of Optical Tomography, Photon Migration, and Spectroscopy of Tissue and Model Media: Theory, Human Studies, and Instrumentation*, B. Chance and R. R. Alfano, eds., Proc. SPIE **2389**, 669–681 (1995).
11. G. Strang, *Linear Algebra and Its Applications*, 3rd ed. (Harcourt Brace Jovanovitch, San Diego, Calif., 1988), Chap. 5, pp. 269–272.
12. G. Strang, *Linear Algebra and its Applications*, 3rd ed. (Harcourt Brace Jovanovitch, San Diego, Calif., 1988), Chap. 7, pp. 370–372.
13. F. S. Acton, *Numerical Methods That Work*, 2nd printing (Mathematical Association of America, Washington, D.C. 1990), Chap. 8, pp. 211–220.
14. K. Furutsu and Y. Yamada, "Diffusion approximation for a dissipative random medium and the applications," Phys. Rev. E **50**, 3634–3640 (1994).
15. A. H. Gandjbakhche, R. F. Bonner, R. Nossal, and G. H. Weiss, "Absorptivity contrast in transillumination imaging of tissue abnormalities," Appl. Opt. **35**, 1767–1774 (1996).
16. F. H. Schlereth, J. M. Fossaceca, A. D. Keckler, and R. L. Barbour, "Imaging in diffusing media with a neural net formulation: A problem in large scale computation," in *Proceedings of Physiological Monitoring and Early Detection Diagnostic Methods*, T. S. Mang, ed., Proc. SPIE **1641**, pp. 46–57 (1992).
17. At each surface, the partial sums of Eq. (4.A.1) must be computed in a specific manner to ensure that the boundary condition is satisfied. The nth partial sum for a reflected flux consists of the $i = 0, \pm 1, \ldots, \pm n$ terms, while the nth partial sum for a transmitted flux is the sum of the $i = 0, \pm 1, \ldots, \pm(n-1), +n$ terms. Under this procedure, the calculated $|\mathbf{J}(x, 0, 0)|$ arising from the source at depth z_0 is nearly equal to the $|\mathbf{J}(x, 0, Z)|$ arising from the source at $Z - z_0$, as expected.
18. W. H. Press, S. A. Teukolsky, W. T. Vetterling, and B. P. Flannery, *Numerical Recipes in* FORTRAN, 2nd ed. (Cambridge U. Press, New York, 1992), Chap. 15, pp. 678–683.
19. *PSI-Plot™ Version 4 for Windows™ User's Handbook* (Poly Software International, Salt Lake City, Utah, 1995), Chap. 5, p. 148.
20. R. E. Alcouffe, Group XTM, Los Alamos National Laboratory, Los Alamos, N. M. 87545 (personal communication, 1995).
21. J. J. Duderstadt and W. R. Martin, *Transport Theory* (Wiley, New York, 1979), Chap. 2, pp. 69–72.
22. E. Beltrami, *Mathematical Models in the Social and Biological Sciences* (Jones and Bartlett, Boston, Mass., 1993), Chap. 1, pp. 1–19.
23. F. A. Grünbaum, "Diffuse tomography: the isotropic case," Inverse Probl. **8**, 409–419 (1992).
24. A. Q. Howard, Jr., W. C. Chew, and M. C. Moldoveanu, "A new correction to the Born approximation," IEEE Trans. Geosci. Remote Sens. **28**, 394–399 (1990).
25. S. R. Arridge, M. Schweiger, M. Hiraoka, and D. T. Delpy, "Performance of an iterative reconstruction algorithm for near infrared absorption and scatter imaging," in *Proceedings of Photon Migration and Imaging in Random Media and Tissues*, B. Chance and R. R. Alfano, eds., Proc. SPIE **1888**, pp. 360–371 (1993).